www.elsevier.com/locate/csr

Impact of sediment-induced stratification and turbulence closures on sediment transport and morphological modelling

Laurent O. Amoudry, Alejandro J. Souza

PII: S0278-4343(11)00079-3
DOI: doi:10.1016/j.csr.2011.02.014
Reference: CSR 2341

To appear in: *Continental Shelf Research*

Received date: 16 June 2010
Revised date: 10 February 2011
Accepted date: 21 February 2011

Cite this article as: Laurent O. Amoudry and Alejandro J. Souza, Impact of sediment-induced stratification and turbulence closures on sediment transport and morphological modelling, *Continental Shelf Research*, doi:10.1016/j.csr.2011.02.014

Impact of sediment-induced stratification and turbulence closures on sediment transport and morphological modelling

Laurent O. Amoudry*,[a], Alejandro J. Souza[a]

[a]National Oceanography Centre, Joseph Proudman Building, 6 Brownlow Street, Liverpool, L3 5DA, UK

Abstract

Appropriate descriptions of turbulence are important in predicting sediment transport and seabed evolution. We use here a three-dimensional model to investigate the impacts of sediment-induced stratification, erosion parameterization, and turbulence closures on sediment transport and morphological simulations. The model is implemented in the Proudman Oceanographic Laboratory Coastal Ocean Modelling System (POLCOMS), which couples a hydrodynamic model to the General Ocean Turbulence Model (GOTM) and to a sediment transport model. This sediment transport model calculates both suspended sediment concentrations and bed evolution. A large number of turbulence closures can be tested and we focus on the methods used to calculate the turbulent length scale and the stability functions. Different modelling scenarios are assessed against experimental data of velocity profiles, suspended sediment concentrations, and trench migration in a laboratory flume. Numerical results show that the processes investigated have little impact on the flow velocity profiles, in spite of some differences on the bed shear stress. The only exception is the one-equation turbulence closure, which can not reproduce velocity profiles appropriately. Sediment-induced stratification, erosion parameterization, and turbulence closures can all have significant impacts on the suspended sediment concentration and the bed evolution. Model-data comparisons are found to be particularly sensitive to the method used to calculate the turbulent length scale.

Key words: sediment transport, morphological modelling, turbulence modelling, sediment-induced stratification

1. Introduction

Nearshore and estuarine areas are under increasing pressures and forecasting tools are needed for management, regulation and coastal engineering. This in turn highlights the demand for ever evolving coastal modelling systems. Since sediment transport is a key component in coastal interactions, models representing the fate of particles in the coastal ocean and in estuaries as well as morphological evolution are essential in order to conduct large scale coastal predictions.

*Corresponding author.
Email addresses: laou@pol.ac.uk (Laurent O. Amoudry), ajso@pol.ac.uk (Alejandro J. Souza)

Morphological models applied to coastal problems have seen sustained development in the past few decades. Two-dimensional depth-averaged (2DH) models, to which quasi three-dimensional concepts were often added, were developed for river flows and then used in coastal areas (de Vriend et al., 1993). However, such models have limited applicability and the three-dimensional flow structure has to be described in complex situations. In particular, depth-averaged models do not describe adequately cases for which density gradients are significant, which is common in estuarine and coastal waters (e.g., Burchard et al., 2008). Progressively, along with the increase in available computer resources, fully three-dimensional flow models have been developed. Gessler et al. (1999) reported such an effort for river morphology and three-dimensional models have recently been introduced for coastal situations (e.g., Lesser et al., 2004; Warner et al., 2008).

These models have commonly been tested against several simple benchmark tests. An important one considers the migration of a trench under a steady current and uses the experimental data of van Rijn (1987). This test allows to validate the model's ability to reproduce both suspended sediment concentration profiles and morphological evolution and is usually chosen because of the opportunity to study such processes without complications introduced by wave-current interactions, water density stratification, and mixed sediments. In spite of its simplicity, the flow over a trench is also a good test scenario for hydrodynamic simulations (e.g., Stansby and Zhou, 1998; Christian and Corney, 2004).

A good description of turbulence is fundamental in three dimensional models and numerical results depend on the closure employed. Numerical predictions of stratification in the coastal ocean are impacted by the turbulence closure employed (e.g., Holt and Umlauf, 2008). For the flow over a shallow trench, Christian and Corney (2004) found significant differences for the hydrodynamic results depending on the turbulence closure used. Turbulence modelling may also impact significantly numerical simulations of suspended sediment (e.g., Warner et al., 2005) and the calculation of bed shear stresses (e.g., Puleo et al., 2004), which is critical in estimating sediment transport and morphological evolution. While such results help to address which turbulence closure is best suited for sediment transport, formal assessment of turbulence closures with data of morphological evolution is still lacking. Other processes may also impact significantly sediment transport numerical predictions. Sediment-induced stratification (SIS) is often implemented as an optional process in coastal models, and can affect the movement of coastal morphological features (e.g., Falchetti et al., 2010) as well as turbulence. Sediment bed erosion and sediment deposition may also employ different parameterizations. The numerical results are usually sensitive to empirical parameters such as the critical erosion bed shear stress (e.g., Gerritsen et al., 2000; Harris et al., 2008). Predictions of suspended sediment may also vary depending on the formulations implemented (e.g., Amoudry et al., 2005). It is thus important not only to investigate the impact due to turbulence closures, but also to compare such effect to the impacts due to sediment-induced stratification and erosion parameterization.

To that goal, we use here an advanced coupled hydrodynamics, sediment transport and turbulence model, which is part of the Proudman Oceanographic Laboratory Coastal Ocean Modelling System (POLCOMS).

In this system, a fully three-dimensional hydrodynamic model (Holt and James, 2001) is coupled to a sediment transport module (Amoudry et al., 2009) and to the General Ocean Turbulence Model (GOTM) (Umlauf et al., 2005). Following previous developments of three-dimensional models, we use the migration of a trench under a steady current as a benchmark test case and the experimental data will be used to quantitatively assess the effects considered. We will first provide a description of the model employed. The hydrodynamic component is only briefly summarized in the manuscript and presented in the appendix, while the turbulence and sediment transport models are described in details since they are essential components of the model comparisons undertaken here. We then describe the numerical setup implemented to reproduce the experiments of van Rijn (1987). In sections 4.1, 4.2 and 4.3, results on the effects of sediment-induced stratification, erosion parameterization, and turbulence closure are presented both independently of and in comparison with each other. The mechanisms responsible for the differences observed in the numerical results are then discussed in section 5.

2. Model description

POLCOMS consists of a baroclinic three-dimensional hydrodynamic model that can be used in regions covering both the deep ocean and continental shelves (Holt and James, 2001). It can be coupled to several external models, in particular a wave model (Osuna et al., 2004; Bolanos et al., 2008), GOTM (Holt and Umlauf, 2008), and an ecosystem model (Allen et al., 2001). A sediment transport and morphological model has recently been added to the hydrodynamic model (Amoudry et al., 2009).

2.1. Hydrodynamic model

The hydrodynamic model solves the three-dimensional, hydrostatic, Boussinesq equations of motions. The governing equations can be formulated either in spherical polar coordinates, or in Cartesian coordinates, which we will use here. The vertical coordinate is taken to be $\sigma = (z - \zeta)/(h + \zeta)$, where z is the Cartesian vertical coordinate, h the reference water depth and ζ the elevation above the reference water level. A time-splitting technique is used to calculate barotropic and baroclinic components and the velocities are thus divided into a depth varying and depth independent parts. The equations of motions for both parts have been presented in Holt and James (2001) and Souza and James (1996) and are only summarized here in the appendix.

The turbulent stresses and turbulent fluxes in the depth varying governing equations are modelled following turbulent viscosity and turbulent gradient diffusion hypotheses, which respectively introduce the eddy viscosity and eddy diffusivities. Both quantities require further closure, which is the aim and focus of the turbulence model and is discussed in the next section.

Surface stresses are not considered in the present study. The determination of the bottom stresses is an important part of the sediment transport and near-bed modelling because the bed shear stress explicitly

determines both the bed load transport rate and the erosion rate. In this study, only steady currents are considered and the bottom shear stress is calculated using a drag coefficient expression that relies on a logarithmic velocity profile and leads to the following expression for the stress components F_B and G_B

$$(F_B, G_B) = (u_B, v_B) \left[\frac{\kappa}{\ln(\delta_0/z_0)} \right]^2 \sqrt{u_B^2 + v_B^2} \tag{1}$$

where (u_B, v_B) are the near-bed velocity (velocity of the bottom vertical grid) defined at an elevation δ_0 above the sea bed. $\kappa = 0.41$ is the von Karman constant and z_0 the bed roughness, which is set here as a user-defined constant. In GOTM, the von Karman constant is calculated from the model constants (Umlauf and Burchard, 2003), which leads to values that may differ slightly from 0.41 depending on the model. This has however no effect on the present simulations.

2.2. Turbulence modelling

Since salinity and temperature are not considered in the present application, the turbulence closure really aims at representing the turbulent stresses and turbulent sediment fluxes. Using the turbulent viscosity and turbulent gradient diffusion hypotheses, it does so by calculating eddy viscosity and eddy sediment diffusivity. Two models are implemented directly within POLCOMS: a one equation model solving a balance equation for $q^2 = 2k$ with k being the turbulent kinetic energy and using a parabolic length-scale (Holt and James, 2001), and the two-equation model ($q^2 - q^2 l$) of Mellor and Yamada (1982) as modified by Galperin et al. (1988). For both these models, the eddy viscosity and the sediment diffusivity are respectively given by

$$\nu_t = S_M l q, \quad \text{and} \quad K_z^s = S_s l q. \tag{2}$$

Several other turbulence closures are available by coupling GOTM to POLCOMS (e.g., Holt and Umlauf, 2008). For these closures, the turbulent eddy viscosity and the sediment diffusivity K_z^s are written as

$$\nu_t = c_\mu l \sqrt{k} \quad \text{and} \quad K_z^s = c_\mu^s l \sqrt{k}. \tag{3}$$

For both approaches (equations 2 or 3), l is a length scale and the dimensionless quantities S_M, S_s, c_μ, and c_μ^s are referred to as stability functions. All the models used in the present study solve a balance equation to calculate the energy scale (q^2 or k) and they all limit the turbulent length scale following Galperin et al. (1988):

$$l \leq 0.53 \frac{q}{N} \tag{4}$$

where N is the buoyancy frequency and is defined in the next section. Different methods are used to calculate l and different formulations are implemented for the stability functions.

2.2.1. One-equation model

A one-equation model is implemented within the POLCOMS hydrodynamic model. It follows equation 2. The velocity scale is found by solving a balance equation and the length scale is prescribed algebraically. The balance equation for q^2 is given by

$$\frac{\partial q^2}{\partial t} = T(q^2) + \mathcal{P}_q + \mathcal{G}_q - \varepsilon_q \tag{5}$$

where $T(q^2)$ represents the diffusive transport term (see equation 37) with the diffusivity for q given by $K_z^q = S_q l q$. $\mathcal{P}_q = 2\nu_t M^2$ is the shear production, $\mathcal{G}_q = -2K_z^s N^2$ is the buoyancy production, and $\varepsilon_q = 2q^3/16.6l$ is the turbulence dissipation rate. The squares of the shear and buoyancy frequencies are respectively

$$M^2 = H^{-2}\left[\left(\frac{\partial u}{\partial \sigma}\right)^2 + \left(\frac{\partial v}{\partial \sigma}\right)^2\right], \tag{6}$$

and

$$N^2 = H^{-1}\frac{\partial b}{\partial \sigma}. \tag{7}$$

where b is the buoyancy and $H = h + \zeta$. These two quantities yield the gradient Richardson number $Ri = N^2/M^2$.

The length scale is specified algebraically and follows Holt and James (2001) by taking

$$l = \kappa H\left(1+\sigma\right)\left(-\sigma\right)^{0.5}. \tag{8}$$

2.2.2. Two-equation models

Several two-equation models can be chosen either directly within POLCOMS or through coupling with GOTM. They all solve one balance equation for the turbulent energy (q^2 or k) and a second one to obtain the turbulent length scale. Even though the $q^2 - q^2 l$ model of Mellor and Yamada (1982) as modified by Galperin et al. (1988) is implemented in POLCOMS and GOTM, it was found to lead to solutions that diverged to unrealistic strong turbulent diffusivities. It is therefore not further discussed in the present study.

The $k-\varepsilon$ model (Rodi, 1987) and the $k-\omega$ model (Umlauf and Burchard, 2003) are available through coupling with GOTM. These models use equation 3 and the turbulent kinetic energy k is the solution of the following balance equation

$$\frac{\partial k}{\partial t} = T(k) + \mathcal{P} + \mathcal{G} - \varepsilon \tag{9}$$

where $\mathcal{P} = \nu_t M^2$ and $\mathcal{G} = -K_z^s N^2$ are respectively the shear and buoyancy productions. ε is the turbulent dissipation rate.

The $k-\varepsilon$ model then solves a balance equation for ε

$$\frac{\partial \varepsilon}{\partial t} = T(\varepsilon) + \frac{\varepsilon}{k}\left(C_{\varepsilon 1}\mathcal{P} + C_{\varepsilon 3}\mathcal{G} - C_{\varepsilon 2}\varepsilon\right), \tag{10}$$

while the $k-\omega$ model considers the balance of the inverse turbulent time scale $\omega \equiv \varepsilon/k$, originally formulated by Wilcox (1988) and extended to oceanographic applications by Umlauf et al. (2003):

$$\frac{\partial \omega}{\partial t} = T(\omega) + \frac{\omega}{k}\left(C_{\omega 1}\mathcal{P} + C_{\omega 3}\mathcal{G} - C_{\omega 2}\varepsilon\right) \tag{11}$$

The diffusivities in the $T(.)$ transport terms (see equation 37) are taken to be $K_z^k = \nu_t/\sigma_k$, $K_z^\varepsilon = \nu_t/\sigma_\varepsilon$, and $K_z^\omega = \nu_t/\sigma_\omega$. Both models are fully closed by setting the model constants as summarised in table 1. Exact values for $C_{\varepsilon 3}$ or $C_{\omega 3}$ depend on the choice of stability function and are calculated following Umlauf et al. (2003) with a steady state gradient Richardson number of $Ri_{st} = 0.25$. This so-called steady state gradient Richardson number is the value at which homogeneous turbulence with constant shear and constant stable stratification is in equilibrium. For $Ri > Ri_{st}$, turbulence decays due to stable stratification. For $Ri < Ri_{st}$, turbulence increases due to shear instabilities.

All balance equations for turbulence quantities neglect the advective terms and the horizontal diffusion (Holt and Umlauf, 2008), based on the boundary layer approximation following which horizontal scales are much larger than vertical scales. We will discuss this assumption further with respect to the numerical results in the discussion and conclusion.

2.2.3. Stability functions

For the one-equation model, the stability functions S_M, S_s, and S_q are taken after Galperin et al. (1988):

$$\begin{aligned} S_M &= \frac{0.3933 - 3.086G}{(1-34.68G)(1-6.127G)}, \\ S_s &= \frac{0.4939}{1-34.68G}, \\ S_q &= 0.2 \end{aligned} \tag{12}$$

with $G = -l^2N^2/q^2$.

For the two two-equation turbulence models in GOTM, the stability functions c_μ and c_μ^s can either be constant, empirical functions, or can result from higher-order turbulence models under some simplifying assumptions. Three choices are available for empirical stability functions following Munk and Anderson (1948), Eifler and Schrimpf (1992), or Schumann and Gerz (1995). All three empirical formulations set $c_\mu = c_\mu^0$ as a constant and take c_μ^s as a function of the gradient Richardson number Ri. For the Munk and Anderson (1948) formulation, this function is given by

$$\begin{aligned} c_\mu^s &= \frac{c_\mu^0}{Pr_0}\frac{(1+10Ri)^{1/2}}{(1+3.33Ri)^{3/2}}, \quad Ri \geq 0 \\ c_\mu^s &= c_\mu^0, \quad Ri < 0 \end{aligned} \tag{13}$$

For the Eifler and Schrimpf (1992) approach, we have

$$c_\mu^s = \frac{c_\mu^0}{Pr_0}\left[\left(\frac{c_\mu^0}{Pr_0}Ri + 1\right)^{1/2} - \frac{c_\mu^0}{Pr_0}Ri\right] \tag{14}$$

And finally for the Schumann and Gerz (1995) expression, c_μ^s is related to c_μ through a turbulent Prandtl number (i.e., $c_\mu^s = c_\mu^0/Pr$), which is a function of the gradient Richardson number

$$Pr = Pr_0 \exp\left(-\frac{Ri}{Pr_0 Ri_\infty}\right) - \frac{Ri}{Ri_\infty} \tag{15}$$

with $Ri_\infty = 0.25$. All three formulations require the specification of c_μ^0 and Pr_0 (summarized in table 2), which are preset for Eifler and Schrimpf (1992) and can be set by the user for Munk and Anderson (1948) and Schumann and Gerz (1995).

In addition to constant and empirical stability functions, the third approach results from the solution of simplified forms of full Reynolds Stress Models. Even though such models solve balance equations for the Reynolds stresses and as such cannot be reduced to eddy viscosity and diffusivity forms for the turbulent stresses and turbulent fluxes, they can be simplified following an approximation of the transport terms. This leads to Reynolds stresses being obtained by solving a linear system of algebraic equations (e.g., Umlauf and Burchard, 2005) in so-called Algebraic Reynolds Stress Models (ARSM). Further simplification following the boundary layer approximation then results in formulations for the turbulent stresses and turbulent fluxes that are similar to that of the turbulent eddy viscosity and gradient diffusion hypotheses (Burchard and Bolding, 2001). The vertical diffusivities are then a consequence of the model and the stability functions can be shown to be function of the shear number and the buoyancy number (e.g., Umlauf and Burchard, 2005)

$$\alpha_M = \frac{k^2}{\varepsilon^2} M^2 \quad \text{and} \quad \alpha_N = \frac{k^2}{\varepsilon^2} N^2 \tag{16}$$

A quasi-equilibrium state, which is defined as the state where production and dissipation are in balance, is also used to further simplify the stability functions leading to expressions that depend on the Richardson number only. A number of model constants that depend on the ARSM employed are associated with such implementation of the stability functions. In the present study, we choose to use the constants associated with both versions of the model described in Canuto et al. (2001).

2.3. Sediment transport model

The sediment transport model follows the description of Amoudry et al. (2009). Different sediment transport modules yield outputs such as suspended sediment concentration (SSC) and bed location that are in turn used in the hydrodynamic and turbulence models. An unlimited number of non-cohesive sediment classes can be prescribed. Each sediment class is defined by values for the sediment particle density ρ_s, the sediment particle diameter d, a critical shear stress for erosion τ_{ce} and an erodibility constant E_0. We follow the bed representation of Warner et al. (2008), in which a layered structure is implemented as the sediment bed and only the top bed layer interacts with the bottom flow grid (figure 1). The number of layers characterizing the sediment bed is user-defined and each layer is described by a spatially and time varying thickness, sediment-class distribution, and porosity (ϕ).

2.3.1. Suspended load transport

For each class, the suspended sediment concentration follows an advection-diffusion equation

$$\frac{Dc}{Dt} = T(c) + \frac{W_s}{H}\frac{\partial c}{\partial \sigma} + S_c \tag{17}$$

where S_c is a sediment source/sink term. W_s is the sediment settling velocity and is determined from the sediment and fluid parameters following the van Rijn (1993) formula.

The effect of suspended sediment on the fluid density may be accounted for by summing the contribution of each sediment class:

$$\rho = \rho_w + \Sigma c\,(\rho_s - \rho_w) \tag{18}$$

where ρ is the density of the fluid-sediment mixture, ρ_w the density of the fluid alone ($\rho_w = \rho_0$ here but could be a function of temperature and salinity in other more complicated cases) and c the volumetric suspended sediment concentration for a given class.

At the free surface, the vertical flux of sediment is set to vanish. At the bottom boundary (sediment bed), the vertical flux of sediment is taken to be equal to the sum of erosion E and deposition D. This condition is implemented by including erosion and deposition as a source/sink term for the bottom grid of the water column and preventing advective and diffusive fluxes into the bed. Deposition is due to gravitational settling and is considered to occur for all bed shear stresses ($D = \rho_s W_s c$). Two approaches have been implemented to represent the erosion flux. It can be taken to be directly related to the excess bed shear stress via a linear dependence: (e.g., Ariathurai, 1974):

$$E = E_0(1-\phi)\left(\frac{\tau_b}{\tau_{ce}} - 1\right) \tag{19}$$

where E_0 is the user-defined erodibility constant, ϕ is the top bed layer porosity and τ_b the bed shear stress magnitude. The erosion flux may also be determined from a reference concentration approach (e.g., Garcia and Parker, 1991) $E = \rho_s(1-\phi)W_s c_{ref}$. The reference concentration is usually expressed as empirical or semi-empirical functions of bed shear stress, and we choose here to use the van Rijn (2007b) formula

$$c_{ref} = 0.015\frac{d}{z_{ref}}\frac{(\theta/\theta_{cm} - 1)^{1.5}}{d_\star^{0.3}} \tag{20}$$

where $\theta = \tau_b/(\rho_s - \rho)gd$ is the non-dimensional bed shear stress, θ_{cm} is the critical non-dimensional bed shear stress for initiation of motion according to Shields, $d_\star = d[(\rho_s/\rho - 1)g/\nu^2]^{1/3}$. g is the acceleration of gravity and ν the water kinematic viscosity. The reference level is chosen as $z_{ref} = 20d$ with a minimum value of 1 cm and θ_{cm} is estimated numerically following van Rijn (1984a). In both cases, the erosion is limited by the amount of sediment available in the top bed layer, which is enforced to be at least as thick as the active bed layer of Harris and Wiberg (2001)

$$\delta_a = \max\left[0.007\rho_w\left(\tau_b - \overline{\tau_{ce}}\right), 0\right] + 6\bar{d} \tag{21}$$

where δ_a is the thickness of the active layer and the overbar denotes an average over all sediment classes.

Equations 19 and 20 have traditionally been used for cohesive sediments and non-cohesive sediments respectively. Recent studies have however implemented equation 19 for non-cohesive sediments with success (e.g., Warner et al., 2008). Equation 19 can also be thought of as similar to a linear reference concentration formula (Amoudry and Liu, 2010). For a given particle diameter, the differences between the two approaches concern the power dependence on the excess shear stress and the numerical values of the free parameters. The reference concentration approach as implemented does not present any free parameter, while both E_0 and τ_{ce} are free parameters in equation 19. The direct specification of the erosion flux may then offer greater flexibility but needs to be determined through model-data comparisons for example.

The $T(c)$ term is the sediment diffusion transport term and is closed using the turbulence model. It is interesting to notice that in the present case the specification of the stability functions implicitly determines the Schmidt number, which is the ratio of momentum diffusivity over sediment diffusivity. Here, this results in the Schmidt number being a function of both shear, through M^2, and the concentration gradient, through N^2, whichever empirical or second-order approach is used to calculate the stability functions.

2.3.2. Bed load transport

Sediment motion is initiated when the moments of the driving forces exceed the stabilizing moments. Grains then roll, slide, and jump along the bed resulting in bed load transport. If the lift forces exceed the grain weight, particles may be entrained into suspension. This results in critical values for the bed shear stress required to initiate motion (τ_{cm}) and suspension (τ_{ce}). These critical stresses can be estimated as functions of particle size (e.g., van Rijn, 1984b) and usually define three regimes: no motion, bed load only, and combined suspended and bed loads. For small particles ($d_\star$ less than about 3), the two critical stresses are almost equal and the bed load only regime vanishes.

Bed load capabilities have been implemented in the sediment transport model following a power relationship to the bed shear stress which has been modified to take into account local bed slope effects (Amoudry et al., 2009). The multiplicative constant to the power relationship can vary by up to an order of magnitude and is left as a user input. In spite of its widespread use, this method is based on measurements for which uncertainty is generally not small and limited to grains of diameter larger than 200 to 300 μm (Amoudry and Souza, 2011). For finer particles, bed load predictive power is uncertain at best, and detailed numerical results under the sheet flow regime seem to indicate that traditional formulations overestimate bed load transport rate (Amoudry and Liu, 2010). Instead, for these fine particles, most of the the transport occurs in the suspended load (van Rijn, 2007a).

In addition to the high uncertainty associated with the relatively small particle size used in the present study, implementing bed load would also introduce extra modelling issues. Free parameters for the bed load multiplicative constant, the erosion coefficient E_0, and the critical stress for erosion τ_{ce} would need to be

specified. Another consequence would be that the two erosion approaches would then not employ the same critical stress. Instead, we choose to neglect the explicit formulation of bed load transport rate and specify $\tau_{ce} = \tau_{cm}$. This approach has the advantage of reducing the number of free parameters to one as τ_{cm} is estimated following van Rijn (1984a). Motion of sediment is, in effect, still considered for all values of the bed shear stress above τ_{cm}. The most important issue is to estimate which method would result in the smaller uncertainty. Calibration of separated bed load and suspended load would have to rely on the bed load and suspended load transport rate values reported in van Rijn (1987), while our proposed approach would only rely on the total load transport rate value. The experimental results provide the total load transport rate with significantly less uncertainty and we thus believe that our approach will simultaneously be simpler and more accurate. Finally, the reasonable results that we obtained can be considered as a validation that such appraoch may indeed perform well.

2.3.3. Bed evolution

The bed morphology follows approaches previously introduced in Harris and Wiberg (2001) and Warner et al. (2008), and implemented in Amoudry et al. (2009) for the present model. The location of the sediment bed is updated at each barotropic time step following conservation of mass for the bed. The change in bed level Δz_{bed} results in general from the vertical exchange between the top bed layer and the water column (erosion and deposition) and the convergence or divergence of bed load transport rates. Bed load is neglected here, which leads to the following bed level change (also see figure 1):

$$\Delta z_{bed} = \frac{\Delta t}{\rho_s(1-\phi)}\,(E - D) \tag{22}$$

where Δt is the time step. This change in bed level can be scaled up by a morphological factor F_{morph} that allows computations for accelerated bed changes (Lesser et al., 2004). The new bed location is then computed while solving the depth-averaged governing equations and the bottom boundary condition of the vertical velocity is set as the rate of change of the sea floor.

2.4. Numerical solution

The numerical domain is discretized using a B-grid in the horizontal plane (Arakawa, 1972). Both components of the velocity are defined at u-points which are the centres of the computational cells, half a grid-box to the southwest of the points at which all scalars are defined (b-points, corner points of the cells). Sediment transport variables are defined at the b-points (corners of grid cells) to the exception of the output bed load transport rate, the bed shear stress and the bed roughness, all three defined at u-points. The water column is divided into σ levels, which can vary in the horizontal (Holt and James, 2001) to maintain resolution near the surface and the sea bottom.

A detailed description of the numerical solution for the hydrodynamic model is given in Holt and James (2001) and we only aim to summarize here the important features. The depth averaged equations and the

free surface equations are solved using a forward time centred space differencing technique, and, to prevent grid-scale noise, the surface elevations are filtered following Killworth et al. (1991). The advective terms are calculated following a Piecewise Parabolic Method scheme (James, 1996) and the vertical diffusion terms following a fully implicit scheme.

The numerical solution for the sediment transport module is presented in Amoudry et al. (2009), and uses the same techniques as the hydrodynamic model. Advective and settling terms are thus calculated following the PPM scheme and the diffusive terms following the fully implicit scheme.

3. Model validation and numerical setup

The ability of the model to accurately reproduce suspended sediment concentration profiles and morphodynamic evolution was tested and presented in Amoudry et al. (2009). To that end the standard test case from the laboratory experiment of van Rijn (1987) on trench migration under a steady current was employed. It was found that the present model was indeed able to accurately predict flow velocities and suspended sediment concentrations over the trench, and the bed evolution. Here, a series of numerical experiments are conducted to assess the impact of erosion parameterization, sediment-induced stratification, and turbulence closure on predictions of suspended sediment concentration profiles and bed evolution. The same case of flow over a trench and trench migration is used to isolate processes in the absence of waves and stratification. The experimental data (van Rijn, 1987), which provide trench migration for three initial trench slopes and velocity and sediment concentration profiles for the steepest slope, also allow a quantitative assessment of the quality of the numerical results under several modelling assumptions.

We use here the same numerical setup as in Amoudry et al. (2009), which is summarized in table 3 and figure 2. The 30 m long and 0.5 m wide straight channel is represented numerically using a grid size of 0.1 m in both horizontal directions and 20 constant vertical levels. A flow of 0.51 m/s upstream depth-averaged velocity $\bar{U}$ in 0.39 m upstream water depth h_0 is imposed and a no-gradient condition is set upstream for the concentration. No-slip conditions are applied to the lateral walls. The bed slope and a constant sediment bed roughness are determined so that the flow rate remains uniform along the domain. Trenches with initial side slopes of 1/3, 1/7, and 1/10 are excavated in a bed of well-sorted sand of median diameter 160 μm, modelled here as a single class with $d = 160\ \mu m$ and $\rho_s = 2650\ kg/m^3$. Both the suspended sediment and flow velocity are then allowed to reach steady state before the bed evolution is tracked using a morphological factor of 10. Different values for this morphological factor (1 and 10) have been tested and no influence was observed on the results.

Both erosion parameterizations have been employed. Using equation 19 requires values for E_0 and τ_{ce}. The default value for the critical bed shear stress τ_{ce} has been chosen to correspond to τ_{cm} (see section 2.3.2). A default value for E_0 has been chosen based on model-data comparisons of SSC profiles and trench

migrations for the steepest initial trench case. The best value for E_0 depends on the turbulence model chosen and the presence of sediment-induced stratification. We were able to find a good agreement for the $k-\omega$ model with SIS, which leads to the value $E_0 = 0.0082\ kg/m^2/s$, but were unable to obtain satisfactory results for the $k-\varepsilon$ model with SIS (see section 4.2.2) without changing $\tau_{ce} = \tau_{cm}$.

The different characteristics of the numerical experiments conducted are summarized in table 4. Several modelling assumptions and parameterizations can then be assessed from intercomparisons between these experiments. The effects of sediment-induced stratification are studied for two turbulence closures. The impact of modifying the erosion parameterization either via different parameters or different formulations can also be investigated for two different turbulence closures. Two values for E_0 and three values for the critical bed shear stress τ_{ce} are tested. The larger critical stress value corresponds to a non-dimensional value of 0.1 and the smaller value to a non-dimensional value of 0.04. Finally, different turbulence closures are assessed: three differ on the approach employed to calculate the turbulent length scale, and five differ on the stability functions implemented. As mentioned previously, the q^2-q^2l model of Mellor and Yamada (1982) as modified by Galperin et al. (1988) has been found to consistently lead to solutions that diverge to unrealistic strong turbulent diffusivities, and it is thus not discussed further.

4. Numerical results

Results from the numerical experiments in table 4 are investigated independently and compared with each other in this section. We will also compare the values obtained for the upstream bed shear stress (summarized as friction velocity in table 5). Upstream of the trench, the flow should reduce to a simple open channel flow, and the clear flow bed shear stress can thus be estimated analytically from the water depth and the bed slope. While the bed shear stress could be modified for the sediment laden flow, the clear flow value still provides a good reference value. The quality of the trench migration simulations is also assessed numerically via the Brier Skill Score (Sutherland and Soulsby, 2004) in table 6.

$$BSS = 1 - \frac{\sum_i \left(z_{num,i} - z_{exp,i}\right)^2}{\sum_i \left(z_{base,i} - z_{exp,i}\right)^2} \tag{23}$$

where $z_{exp,i}$ are the experimental observation of the bed location, $z_{num,i}$ the corresponding numerical predictions, and $z_{base,i}$ base values usually taken to be the initial condition. All scores are positive as all cases predict a trench migration in the correct direction, and perfect agreement gives a score of 1. Most values remain high, but this skill factor does not provide information on whether trench migration and filling are overestimated or underestimated.

4.1. Impact of sediment-induced stratification on sediment transport model

The effect of sediment-induced stratification is isolated for two turbulence models by comparing experiment S1A with N1A for the $k-\omega$ model, and experiment S2B with N2B for the $k-\varepsilon$ model. The impacts

observed are consistent. As expected, the upstream bed shear stress is reduced when SIS is added (table 5). While this corresponds to a reduced near-bed velocity due to the presence of sediment, the velocity profiles over the trench are not significantly altered by the inclusion or exclusion of the SIS (figure 3). The SSC profiles do show differences due to SIS that are mainly occurring away from the bed and following which there is less suspended sediment when stratification is included. Both reductions of upstream bed shear stress and SSC in the presence of SIS are consistent with how stratification is taken into account in the turbulence closures. The buoyancy production term in the turbulence model is proportional to the concentration gradient for SIS (i.e., $G \propto \partial c/\partial z$). This term is usually negative and results in turbulence damping, which leads to reduced bed shear stresses, reduced vertical mixing of sediment and finally less suspended sediment high in the water column.

While the numerical results obtained in the absence of stratification seem to better match the suspended concentration data (figure 3), the experimental data revealed that the suspended particles had a diameter of 160 μm near the bed, but only 120 μm near the surface (van Rijn, 1987). This effect is not presently included in the model since only one fixed particle diameter is specified. However, the effect of such a particle diameter discrepancy is far from being negligible on the suspended sediment concentration (figure 4). We thus believe that the lack of agreement between SIS simulations and data in figure 3 is probably due to a poor representation of the sand grain size distribution by a single class in the model.

The effect of SIS on the bed evolution is a consequence of the generally smaller bed shear stresses and transport rates under SIS. The trenches do not migrate as far and are not filled as much when stratification is included (figure 5). For example, the amount of downstream migration changes by as much as 15 % (0.5 m out of 3 to 4 metres) for the $k-\omega$ model. The differences in trench filling are more significant and can reach up to a factor two. The overall effect of SIS on trench migration, as measured by the Brier Skill Score in table 6, depends on the turbulence model employed. For the $k-\omega$ model, the impact is small in all cases and neglecting SIS leads to better model-data comparisons in one case. For the $k-\varepsilon$ model, the effect is clearly more pronounced. As mentioned previously and discussed in details in section 4.2.2, no reasonable trench migration could be obtained for the $k-\varepsilon$ model with sediment-induced stratification. This issue of particularly strong and negative effect of SIS for the $k-\varepsilon$ model is not unique to POLCOMS and is also present in the DELFT3D system (Delft Hydraulics (2007), page 11-3).

4.2. Impact of erosion parameterization on sediment transport model

4.2.1. Comparison of bed-flow exchange approaches

The choice of the erosion approach implemented has a significant impact on bed shear stress (table 5), SSC profiles (figure 6), and trench migrations (figure 7). The van Rijn reference concentration approach leads to predictions of severely reduced upstream bed shear stress and higher near-bed concentrations. The bed shear stress reduction is consistent with the effect of sediment stratification following which a stronger near-

bed concentration gradient results in stronger turbulence damping and lower bed shear stress. Compared with the experimental data, the van Rijn reference concentration approach leads to somewhat better results, but generally overpredicts the amount of suspended sediment especially close to the bed. The linear erosion flux approach generally underpredicts the data. Further taking into account the effect of the sediment size distribution (figure 4 and related discussion), this could mean that the van Rijn approach may significantly overpredict the SSC experimental values.

Dramatic differences are found for the trench migrations (figure 7 and table 6). The van Rijn reference concentration approach leads to trench migrations and trench filling that are both much too large. The numerical trench reaches the final state of the experiment in about the tenth of the time (about 1.5 hours versus 15 hours). At the end of the 15 hours, the trench has then entirely filled and migrated out of the numerical domain. Such behaviour is explained by the significantly larger near-bed concentrations which result in much larger sediment fluxes since velocities remain similar (figure 6). While this obviously questions the use of this implementation as specified in section 2.3 (i.e., an off-the-shelf formulation for c_{ref}), the present results do not provide conclusive evidence against the use of the same method with a different c_{ref} formula, or against the use of the specific power relationship in equation 20 independently of all numerical parameters. For example, the 0.015 coefficient was originally determined empirically from flume and field data for sediment of diameters larger than 180 μm, and this value may not be valid in the present case. It may furthermore be possible to obtain good numerical results by having a free parameter to be determined from model-data comparisons instead of the fixed value of 0.015, as in van Rijn (1987).

4.2.2. Sensitivity of numerical results to erodibility constant and critical erosion stress

When the direct erosion flux formulation following equation 19 is chosen, user-defined values for E_0 and τ_{ce} are required. In general, highly precise information on either quantity is not easily obtained, which raises the issue of how sensitive results are to such values. Even though the present model implements $\tau_{ce} = \tau_{cm}$ and thus relies on a known and well-accepted expression of the critical stress as a function of particle size, the value may not be obtained with absolute certainty. Numerical results for cases S1A, S1B, S1C and S1D (figures 8 and 9) help assess the sensitivity to a 35 % change in E_0 and to "worst-case" errors on $\tau_{ce} = \tau_{cm}$. The effect on the bed shear stress (table 5) is small, and velocity profiles are again very similar. The resulting behaviour for the SSC (figure 8) is expected as increasing E_0 and τ_{ce} do respectively lead to more and less suspended sediment. These discrepancies on the SSC appear to be of similar magnitude as those due to stratification, but remain smaller than the changes incurred from modifying the settling velocity via a different particle diameter (figure 4).

The different bed evolutions computed for cases S1A, S1B, S1C and S1D are presented in figure 9. An increase in erodibility causes larger downstream migration and more trench filling. An increase in critical bed shear stress leads to less migration and less filling, and vice versa. The result in absence of sediment-

induced stratification is also included in figure 9 to allow for easy comparison of the different effects. In all cases, the impacts observed due to the changes in E_0 and τ_{ce} are significantly larger than that of neglecting sediment-induced stratification (table 6). Errors in the migrated distance are of the order of one to two metres, and correspond to at least twice the error due to stratification. The effect on the trench infilling is less evident, but still present.

The impacts of E_0 and τ_{ce} are also relevant for the $k-\varepsilon$ model, in particular concerning the difficulty in obtaining reasonable trench migration predictions with sediment-induced stratification. Following from the sensitivity results displayed in figure 9, improving the numerical results for the $k-\varepsilon$ model would require increasing E_0 or decreasing τ_{ce}. The latter could only be justified by uncertainties in the Shields curve or correspondence to a particle size larger than reported in van Rijn (1987). The effect of increasing E_0 or decreasing τ_{ce} for the $k-\varepsilon$ model is shown in figure 10. As expected and consistent with results of figure 9, both do increase how far downstream the trench migrates. However, both parameter changes do not lead to more trench filling, but to the opposite and a deeper final trench. While an absolute conclusion on a complete inability of the $k-\varepsilon$ model to reproduce the trench migration is difficult, good model-data comparisons would require changes to E_0, τ_{ce}, or both, which would hardly be physically justifiable.

4.3. Impact of turbulence modelling on sediment transport model

4.3.1. Turbulence model

While there seems to be a general consensus on the use of a balance equation for k and its form, it is not necessarily the case for the method employed to calculate the turbulent length scale l. We compare here the three models described in section 2.2: the one-equation model hereafter called k model (experiment S3A) and two two-equation models, the $k-\varepsilon$ model (experiment S2A) and the $k-\omega$ model (experiment S1A).

Both two-equation models lead to velocity and SSC profiles displaying little differences (figure 11), and the $k-\omega$ upstream bed shear compares best with the analytical value. The effect of different two-equation models on the SSC profiles is found to be smaller than that of the sediment-induced stratification. While the impact on velocities and bed shear stress may be considered independently of sediment erosion calibration, this is not be the case for the SSC profiles, and the better $k-\omega$ profiles have to be considered cautiously. In comparison, the one-equation model is dramatically not able to reproduce the experimental data. The upstream bed shear stress severely underpredicts the analytical value, and is significantly worse than both two-equation predictions. The velocities predicted by the k model exhibit profiles that are quite different to the $k-\omega$ and $k-\varepsilon$ profiles and that are a very poor match to the data. Finally, the k model fails profoundly in predicting the SSC compared to the two-equation models.

The three different models lead to widely different trench migrations (figure 12). The $k-\omega$ performs relatively well and the k model poorly, both of which can be expected in light of the previous results. The $k-\varepsilon$ model surprisingly performs poorly. While the sediment erosion has been calibrated with the $k-\omega$

model, no physically reasonable value for the sediment erosion parameters was found to lead to good trench migration predictions with the $k-\varepsilon$ model (see section 4.2.2). This model was however found to produce reasonable migrations when neglecting sediment-induced stratification (figure 5). The effect represented in figure 12 is obviously much larger than that of neglecting SIS. Both the k and the $k-\varepsilon$ models underpredict the extent of horizontal migration about equally bad. In addition, they also both do not produce enough trench filling, the $k-\varepsilon$ model being worse (table 6). Finally, while the k model does predict a reasonable bathymetry far downstream (past about 18 metres along the channel), the $k-\varepsilon$ leads to a bathymetry profile that return to the initial unexcavated bed too quickly.

4.3.2. Stability functions

Last, we investigate the effects of the method chosen to calculate the stability functions. While they may not always be negligible, they are indeed small in comparison with some effects already investigated. The main difference occurs between the empirical approaches as a group (experiments S5A, S6A and S7A) and the second-order models as a group (experiments S1A and S4A). The velocity profiles are almost the same for all cases (figure 13) and the upstream bed shear stress shows very little variation between the different experiments (table 5). Some discrepancies can be observed for the SSC between the empirical approaches and the second-order models, the former leading to higher concentrations that are also slightly larger than in the unstratified (N1A) case (figure 13). The effects on the trench migration in figure 14 and table 6 also show the main difference being between empirical approaches and second-order models and being very similar in magnitude to the impact of stratification. Comparison between different empirical approaches or between different second-order models shows negligible impact. Overall, this illustrates that only the choice between empirical formulations or expressions derived from second-order models matters for this particular application.

5. Discussion

The numerical results presented in the previous section expose an important influence of the choice of turbulence model on morphological predictions. While this is not necessarily surprising given previous findings (e.g., Puleo et al., 2004; Warner et al., 2005), it requires further explanation and discussion. The mediocrity of the one-equation k model is not unexpected. This turbulence model is indeed inherently flawed as being highly empirical and flow dependent (e.g., Pope, 2000). In particular, the algebraic length scale expression that is valid for a given flow may not be appropriate to describe the turbulence in other more complicated situations.

The justification for discrepancies between two-equation models is however less evident. Figure 15 presents numerical results of the bed shear stress, erosion, and deposition along the channel at the start of the morphological computations for the $k-\varepsilon$ and $k-\omega$ models, both with sediment-induced stratification.

Upstream of the trench, the bed shear stresses are not identical and the $k-\varepsilon$ value is smaller (see also table 5). For both models, erosion and deposition are in equilibrium. Over the trench, the flow deceleration results in the bed shear stress first reducing sharply before increasing slowly to reach a constant value at the end of the trench. Downstream of the trench, the flow acceleration leads to a peak in bed shear stress. For both the channel deepening and the end of the trench, the $k-\varepsilon$ model results in bed shear stress that relaxes more quickly to the "far-downstream" value. In turn, such behaviour for the bed shear stress leads to differences in the balance between erosion and deposition. In the trench, both models give no erosion just after the deepening as the bed shear stress falls below the critical value τ_{ce}, then the higher bed shear stress values for the $k-\varepsilon$ model lead to stronger erosion. Simultaneously, the deposition flux in the trench is reduced from the upstream value, which leads to lower values for the $k-\varepsilon$ model. These combined patterns of erosion and deposition result in net deposition throughout the trench for the $k-\omega$ model, but not for the $k-\varepsilon$ model, for which an erosion zone can be distinguished in the middle of the trench. This explains the observation of deeper final trenches for increased E_0 values in figure 10. Downstream of the trench, the numerical results lead to net erosion for the $k-\omega$ model, and net erosion followed by deposition for the $k-\varepsilon$ model. Overall, the $k-\omega$ model results in relatively simple pattern of bed accretion followed by net bed erosion. In comparison, the combination of (i) lower upstream bed shear stress and (ii) faster return to uniformity of the $k-\varepsilon$ model lead to more complicated and lower intensity successions of accretion and bed erosion zones. In turn, these result in less perceived trench migration and in a deeper final trench.

A remaining important issue then concerns the fundamental difference between the two two-equation models. Physically, the $k-\varepsilon$ and $k-\omega$ models are based on the same cascading relation for the turbulence dissipation, and should be equivalent. However, this equivalence may not be assured in mathematical terms. The ω equation implied by the modelled ϵ equation (equation 10) is

$$\frac{\partial \omega}{\partial t} = \frac{T(\varepsilon)}{k} - \frac{\varepsilon}{k^2} T(k) + \frac{\omega}{k} \left[\left(C_{\varepsilon 1} - 1 \right) \mathcal{P} + \left(C_{\varepsilon 3} - 1 \right) \mathcal{G} - \left(C_{\varepsilon 2} - 1 \right) \varepsilon \right]. \tag{24}$$

The $k-\varepsilon$ model and the $k-\omega$ model are thus mathematically equivalent if the model constants satisfy

$$C_{\omega 1} = C_{\varepsilon 1} - 1 \tag{25}$$

$$C_{\omega 2} = C_{\varepsilon 2} - 1 \tag{26}$$

$$C_{\omega 3} = C_{\varepsilon 3} - 1 \tag{27}$$

and if the diffusive terms follow

$$T(\omega) = \frac{T(\varepsilon)}{k} - \frac{\varepsilon}{k^2} T(k) \tag{28}$$

It is worthwhile noting that the advective terms are physically and mathematically exactly identical in all models. Neglecting them does not change any of the right-hand side terms in equations 9, 10, 11 and 24;

only the left-hand side term changes to from $\partial/\partial t$ to D/Dt. Advective processes will thus not generate discrepancies between different models, even if they can transport differences that are already introduced.

The relationship between the model constants can be assessed from table 1 for the shear production and dissipation terms. The constants related to the buoyancy production are calculated following the constraint discussed in Umlauf et al. (2003), which leads to $C_{\omega 3} = -0.642$ and $C_{\varepsilon 3} = -0.629$ for the stability functions from Canuto et al. (2001). Equations 25 and 26 are indeed close to be satisfied, which should only induce minor differences between the $k-\varepsilon$ model and the $k-\omega$ model. Equation 27 is not satisfied. Physically, the values for $C_{\omega 3}$ and $C_{\varepsilon 3}$ mean that the buoyancy term would act in opposite ways in the turbulence dissipation rate balance. While this could help explain the particular issues encountered by the $k-\varepsilon$ model in combination with sediment-induced stratification, the gradient Richardson number observed in the numerical results always remains small (less than 0.1). Turbulence in the stratified flow is thus controlled by shear instabilities and changes to the buoyancy production term should not lead to significant impacts on the results. We confirmed this by changing the $C_{\varepsilon 3}$ value to 0.358 and only finding a small impact of the trench migration. The model constants chosen are thus not the cause of the important differences observed in the morphological computation.

The closure of the diffusive terms is the other primary source of discrepancies between the models. Equation 28 is assessed in figure 16 at the five locations across the trench that have been used for model-data comparison previously. The left-hand side and the right-hand side terms of equation 28 cannot be considered to be equal. This is particularly prounounced near the sediment bed and confirms that the diffusive terms in the $k-\varepsilon$ and $k-\omega$ models are not equivalent. The resulting additional term has been referred to as a cross-diffusion term and discussed for boundary layers in Wilcox (1993), where it has been related to the rate of increase of l. In the present study, the $k-\omega$ turbulence length scale is larger than the $k-\varepsilon$ value when $T(\omega) < \frac{T(\varepsilon)}{k} - \frac{\varepsilon}{k^2}T(k)$ close to the bed (first and last profiles in figure 16), and vice versa (second and third profiles in figure 16). This difference on the diffusion terms is further compounded by the different values that are taken for σ_k (table 1).

6. Conclusions

We have applied a coupled hydrodynamics, turbulence and sediment transport to a classical test scenario in order to investigate the effects that several modelling approaches have on numerical predictions of sediment transport and morphological evolution. Some important simplifications have been assumed throughout the study. In particular, we use a hydrostatic model and neglect advection of turbulent quantities. The validity of these assumptions is related to the value of the trench slope. For the two gentle slopes, we expect the hydrostatic model to perform reasonably well compared with a non-hydrostatic model (e.g., Stansby and Zhou, 1998) and the horizontal length scale is reasonably large with respect to the vertical one. This is

however not the case for the steepest case and both assumptions may be the source of numerical errors. This may help explain the relatively poor results obtained for the velocity profiles, which would probably be better predicted by a non-hydrostatic model. Such a model would help to better reproduce the recirculating pattern near the upstream trench edge (e.g., Stansby and Zhou, 1998), and higher accuracy of the $k-\omega$ model in this situation is well documented (e.g., Wilcox, 1993). However, flow errors due to steep changes in bathymetry will be mitigated in morphological predictions by the natural sediment transport response which leads to more gentle slopes. Even though a more comprehensive assessment of the effect of the hydrostatic assumption on the numerical bed evolution may be justified, the present model has been able to match reasonably well the experimental data in some cases.

We have investigated the effects of sediment-induced stratification, different erosion parameterizations, and turbulence closures on the numerical results. These effects lead to modifications that are often not negligible, in particular for the bed evolution. Most numerical experiments undertaken predict very similar velocity profiles in spite of differences in the bed shear stress that can be significant. Discrepancies are observed for the suspended sediment concentration profiles, and significant changes are found for the morphological predictions, even for this simple idealized scenario. Even though the Brier Skill Scores remain in general relatively high, the extent of horizontal migration can vary by more than one metre, corresponding to a 25 to 30 % error, and the amount of trench filling can vary by up to a factor two. This illustrates a high sensitivity of morphological predictions to a number of modelling parameterizations. This is in turn a severe limitation to the predictive power of morphological models, even for this simple idealized scenario. For more complex situations, the model sensitivity shown here highlights the crucial need of thorough hindcasting.

Observed underpredictions of the suspended sediment concentration in a number of cases may be due to a poor representation of the sediment size. The overall sediment transport problem should thus be modelled using more than one class of fixed particle size, even for the present simple case. This leads to a series of inferred issues. One concerns how many sediment classes are needed and others relate to the erosion parameterization. Using equation 19 requires the specification of sediment parameters that are not easily determined and to which the numerical results are sensitive. While this can be seen as an important advantage for only one sediment class, it may prove difficult to determine such parameters for more classes. Another approach is to use an "off-the-shelf" formulation devoid of free parameters, such as the van Rijn (2007b) reference concentration, which was not found to be a viable alternative here.

In the present study, the erosion parameterization presented the most dramatic impact on the predictions of sediment transport and bed evolution. However, several other erosion formulations exist and erosional parameters can exhibit significant variability, in particular under field conditions. This makes precise and quantitative comparisons of the different impacts investigated with respect to that of the erosion parameterization difficult. In effect, little more than a qualitative assessment that the erosion parameterization has the most dramatic effect can be made.

Sediment-induced stratification and turbulence closures are clearly interrelated. Sediment-induced stratification directly impacts the turbulence closure through the buoyancy production term, while turbulence closures impact vertical mixing and the level of suspended sediment, thus stratification. The method used to calculate the turbulence length scale is the crucial issue, as it leads to the largest discrepancies. In addition to consistently leading to poor results for hydrodynamics, sediment transport and bed evolution, the one-equation model is not complete since it requires a flow-dependent specification for the length scale (e.g., Wilcox, 1993; Pope, 2000). In contrast, two-equation models are indeed complete. In this application, the $k-\omega$ model has been found to lead to better numerical results than the $k-\varepsilon$ model, in particular for the morphological predictions. The main source of discrepancy between the two two-equation models has been found to be the closure of the diffusion terms. The method employed to calculate the stability functions is found to have a small impact here. The only noticeable difference is between empirical formulations and expressions derived from second-order models, and the specific method within each of these two global approaches seems to be interchangeable.

Acknowledgments

The authors wish to thank L. Umlauf and an anonymous reviewer for their comments, which greatly improved the manuscript. The authors wish to acknowledge the support of the Natural Environment Research Council to the National Oceanography Centre through the Oceans 2025 Research Program and the FORMOST project (NE/E015026/1).

A. Hydrodynamic model description

We summarize here the governing equations of motion for the hydrodynamic model in Cartesian coordinates. The velocities are divided into depth-varying and depth-independent parts, respectively $u = \bar{u}(x,y,t) + u_r(x,y,\sigma,t)$ and $v = \bar{v}(x,y,t) + v_r(x,y,\sigma,t)$. Surface stresses are neglected and the atmospheric pressure is constant. The depth averaged equations are

$$\frac{\partial \bar{u}}{\partial t} = f\bar{v} - g\frac{\partial \zeta}{\partial x} - \frac{F_B}{H} + NLB_x \tag{29}$$

and

$$\frac{\partial \bar{v}}{\partial t} = -f\bar{u} - g\frac{\partial \zeta}{\partial y} - \frac{G_B}{H} + NLB_y \tag{30}$$

The equation for the free surface is

$$\frac{\partial \zeta}{\partial t} = -\frac{\partial H\bar{u}}{\partial x} - \frac{\partial H\bar{v}}{\partial y} \tag{31}$$

The depth varying governing equations are

$$\begin{aligned}\frac{\partial u_r}{\partial t} &= -L(u) + fv_r + T(u) + \frac{F_B}{H} \\ &\quad -\frac{\partial \psi}{\partial x} - \left(\frac{\partial \zeta}{\partial x} + \sigma \frac{\partial H}{\partial x}\right) b - NLB_x \end{aligned} \tag{32}$$

and

$$\begin{aligned}\frac{\partial v_r}{\partial t} &= -L(v) - fu_r + T(v) + \frac{G_B}{H} \\ &\quad -\frac{\partial \psi}{\partial y} - \left(\frac{\partial \zeta}{\partial x} + \sigma \frac{\partial H}{\partial x}\right) b - NLB_y \end{aligned} \tag{33}$$

In these equations, f is the Coriolis parameter, $H = h + \zeta$ is the total water depth, F_B and G_B are the two components of the bottom stresses. $L(.)$, $T(.)$, and $NLB_{x,y}$ are respectively the advective, diffusive, and the depth averaged non-linear and buoyancy terms. The buoyancy is $b = g\left(\rho_0 - \rho\right)/\rho_0$, where $\rho_0 = 1000 kg/m^3$ is a reference density. ψ then relates to the buoyancy following

$$\psi = H \int_0^\sigma b d\sigma \tag{34}$$

The advective terms are expressed following

$$L(a) = u\frac{\partial a}{\partial x} + v\frac{\partial a}{\partial y} + \Omega \frac{\partial a}{\partial \sigma} \tag{35}$$

where the vertical velocity Ω is found by

$$\begin{aligned}\Omega &= -\frac{\sigma}{H}\frac{\partial \zeta}{\partial t} \\ &\quad -\frac{1}{H}\left[\frac{\partial}{\partial x}\left(H\int_0^\sigma u d\sigma\right) + \frac{\partial}{\partial y}\left(H\int_0^\sigma v d\sigma\right)\right] \end{aligned} \tag{36}$$

The vertical turbulent diffusion terms are given by

$$T(a) = \frac{1}{H^2}\frac{\partial}{\partial \sigma}\left(K_z^a \frac{\partial a}{\partial \sigma}\right) \tag{37}$$

where K_z^a is either the eddy viscosity or eddy diffusivity.

References

Allen, J. I., Blackford, J., Holt, J., Proctor, R., Ashworth, M., Siddorn, J., 2001. A highly spatially resolved ecosystem model for the North West european continental shelf. SARSIA 86 (6), 423–440.

Amoudry, L., Hsu, T.-J., Liu, P. L.-F., 2005. Schmidt number and near-bed boundary condition effects on a two-phase dilute sediment transport model. J. Geophys. Res. 110 (C09003).

Amoudry, L. O., Liu, P. L.-F., 2010. Parameterization of near-bed processes under collinear wave and current flows from a two-phase sheet flow model. Cont. Shelf Res. 30, 1403–1416.

Amoudry, L. O., Souza, A. J., 2011. Deterministic coastal morphological and sediment transport modeling. a review and discussion. Rev. Geophys. minor revisions.

Amoudry, L. O., Souza, A. J., Holt, J. T., 2009. Sediment transport module for a B-grid coastal shelf ocean model. In: Mizuguchi, M., Sato, S. (Eds.), Proceedings of Coastal Dynamics 2009: Impacts of Human Activities on Dynamic Coastal Processes. World Scientific.

Arakawa, A., 1972. Design of the UCLA general circulation model. Tech. Rep. 7, Univ. of Calif., Los Angeles.

Ariathurai, C. R., 1974. A finite element model for sediment transport in estuaries. Ph.D. thesis, University of California, Berkeley, USA.

Bolanos, R., Wolf, J., Brown, J., Osuna, P., Monbaliu, J., Sanchez-Arcilla, A., 2008. Comparison of wave-current interaction formulation using the POLCOMS-WAM wave-current model. In: Proceedings of the 31st International Conference on Coastal Engineering.

Burchard, H., Bolding, K., 2001. Comparative analysis of four second-moment turbulence closure models for the oceanic mixed layer. J. Phys. Oceanogr. 31, 1943–1968.

Burchard, H., Flöser, G., Staneva, J. V., Badewien, T. H., Riethüller, R., 2008. Impact of density gradients on net sediment transport into the Wadden Sea. J. Phys. Oceanogr. 38, 566–587.

Canuto, V. M., Howard, A., Cheng, Y., Dubovikov, M. S., 2001. Ocean turbulence. part I: One-point closure model - momentum and heat vertical diffusivities. J. Phys. Oceanogr. 31, 1413–1426.

Christian, C. D., Corney, P. A., 2004. Three dimensional model of flow over a shallow trench. J. Hydrau. Res. 42 (1), 71–80.

de Vriend, H. J., Zyserman, J., Nicholson, J., Roelvink, J. A., Pechon, P., Southgate, H. N., 1993. Medium term 2DH coastal modelling. Coastal Eng. 21, 193–224.

Delft Hydraulics, 2007. Delft3D-FLOW Simulation of multi-dimensional hydrodynamic flows and transport phenomema, including sediments. User manual.

Eifler, W., Schrimpf, W., 1992. ISPRAMIX, a hydrodynamic program for computing regional sea circulation patterns and transfer processes. Tech. Rep. EUR 14856 EN, European Commission Joint Research Center, Ispra, Italy.

Falchetti, S., Conley, D. C., Brocchini, M., Elgar, S., 2010. Nearshore bar migration and sediment-induced buoyancy effects. Cont. Shelf Res. 30, 226–238.

Galperin, B., Kantha, L. H., Hassid, S., Rosati, A., 1988. A quasi-equilibrium turbulent energy model for geophysical flows. J. Atmos. Sci. 45 (1), 55–62.

Garcia, M., Parker, G., 1991. Entrainment of bed sediment into suspension. J. Hydraul. Eng. 117 (4), 414–435.

Gerritsen, H., Vos, R. J., van der Kaaij, T., Lane, A., Boon, J. G., 2000. Suspended sediment modelling in a shelf sea (North Sea). Coastal Eng. 41 (1-3), 317–352.

Gessler, D., Hall, B., Spasojevic, M., Holly, F., Pourtaheri, H., Raphelt, N., 1999. Application of 3D Mobile Bed, Hydrodynamic Model. Coastal Eng. 125 (7), 737–749.

Harris, C. K., Sherwood, C. R., Signell, R. P., Bever, A. J., Warner, J. C., 2008. Sediment dispersal in the northwestern Adriatic Sea. J. Geophys. Res. 113 (C11S03).

Harris, C. K., Wiberg, P. L., 2001. A two-dimensional, time-dependent model of suspended sediment transport and bed reworking for continental shelves. Computers and Geosciences 27, 675–690.

Holt, J., Umlauf, L., 2008. Modelling the tidal mixing fronts and seasonal stratification of the Northwest European continental shelf. Cont. Shelf Res. 28, 887–903.

Holt, J. T., James, I. D., 2001. An s coordinate density evolving model of the northwest European continental shelf 1, model description and density structure. J. Geophys. Res. 106 (C7), 14015–14034.

James, I. D., 1996. Advection schemes for shelf sea models. J. Mar. Syst. 8, 237–254.

Killworth, P. D., Stainforth, D., Webb, D., Paterson, S. M., 1991. The development of a free-surface Bryan-Cox-Semtner ocean model. Journal of Physical Oceanography 21, 1333–1348.

Lesser, G. R., Roelvink, J. A., van Kester, J., Stelling, G. S., 2004. Development and validation of a three-dimensional

morphological model. Coastal Eng. 51 (8-9), 883–915.

Mellor, G., Yamada, T., 1982. Development of a turbulence closure model for geophysical fluid problems. Rev. Geophys. Space Phys. 20 (4), 851–875.

Munk, W. H., Anderson, E. R., 1948. Notes on a theory of the thermocline. J. Mar. Res. 7 (3), 276–295.

Osuna, P., Wolf, J., Ashworth, M. I., 2004. Implementation of a wave-current interaction module for the polcoms system. Tech. Rep. 168, Proudman Oceanographic Laboratory.

Pope, S. B., 2000. Turbulent Flows, 1st Edition. Cambridge University Press, New York.

Puleo, J. A., Mouraenko, O., Hanes, D. M., 2004. One-dimensional wave bottom boundary layer model comparison: Specific eddy viscosity and turbulence closure models. J. Waterw. Port Coastal Ocean Eng. 130 (6).

Rodi, W., 1987. Examples of calculation methods for flow and mixing in statified fluids. J. Geophys. Res. 92 (C5), 5305–5328.

Schumann, U., Gerz, T., 1995. Turbulent mixing in stably stratified flows. J. Appl. Meteorol. 34, 33–48.

Souza, A. J., James, I. D., 1996. A two-dimensional (x-z) model of tidal straining in the Rhine ROFI. Cont. Shelf Res. 16 (7), 949–966.

Stansby, P. K., Zhou, J. G., 1998. Shallow-water flow solver with non-hydrostatic pressure: 2D vertical plane problems. International Journal for Numerical Methods in Fluids 28, 541–563.

Sutherland, J., Soulsby, A. H. P. R. L., 2004. Evaluating the performance of morphological models. Coastal Eng. 51, 917–939.

Umlauf, L., Bolding, K., Burchard, H., 2005. GOTM - Scientific Documentsion. Version 3.2. Marine Science Reports 63, Leibniz-Institute for Baltic Sea Research, Warnemünde, Germany.

Umlauf, L., Burchard, H., 2003. A generic length-scale equation for geophysical turbulence models. J. of Marine Res. 61 (2), 235–265.

Umlauf, L., Burchard, H., 2005. Second-order turbulence closure models for geophysical boundary layers. a review of recent work. Cont. Shelf Res. 25, 795–827.

Umlauf, L., Burchard, H., Hutter, K., 2003. Extending the $k-\omega$ turbulence model towards oceanic applications. Ocean Modelling 5, 195–218.

van Rijn, L. C., 1984a. Sediment transport, part I: Bed load transport. J. Hydraul. Eng. 110 (10), 1431–1456.

van Rijn, L. C., 1984b. Sediment transport, part II: Suspended load transport. J. Hydraul. Eng. 110 (11), 1613–1641.

van Rijn, L. C., 1987. Mathematical modelling of morphological processes in the case of suspended sediment transport. Ph.D. thesis, Delft University of Technology.

van Rijn, L. C., 1993. Principles of Sediment Transport in Rivers, Estuaries and Coastal Seas. Aqua Publications.

van Rijn, L. C., 2007a. Unified view of sediment transport by currents and waves. I: Initiation of motion, bed roughness, and bed-load transport. J. Hydraul. Eng. 133 (6), 649–667.

van Rijn, L. C., 2007b. Unified view of sediment transport by currents and waves. II: Suspended transport. J. Hydraul. Eng. 133 (6), 668–688.

Warner, J. C., Sherwood, C. R., Arango, H. G., Signell, R. P., 2005. Performance of four turbulence closure models implemented using a generic length scale method. Ocean Modelling 8 (1-2), 81–113.

Warner, J. C., Sherwood, C. R., Signell, R. P., Harris, C. K., Arango, H. G., 2008. Development of a three-dimensional, regional, coupled wave, current, and sediment transport model. Computers and Geosciences 34, 1284–1306.

Wilcox, D. C., 1988. Reassessement of the scale-determining equation for advanced turbulence models. AIAA J. 26, 1299–1310.

Wilcox, D. C., 1993. Turbulence modeling for CFD. DCW Industries.

Table 1: $k-\varepsilon$ and $k-\omega$ model constants. The $C_{\varepsilon 3}$ and $C_{\omega 3}$ given result from the Umlauf et al. (2003) constraint with the Canuto et al. (2001) stability functions.

Model	C_μ^0	σ_k	σ_ε, σ_ω	$C_{\varepsilon 1}$, $C_{\omega 1}$	$C_{\varepsilon 2}$, $C_{\omega 2}$	$C_{\varepsilon 3}$, $C_{\omega 3}$
$k-\varepsilon$	0.5477	1.0	1.3	1.44	1.92	-0.629
$k-\omega$	0.5477	2.0	2.0	0.555	0.833	-0.642

Table 2: Stability functions and turbulent Prandtl number constants.

Method	c_μ^0	Pr_0
Munk and Anderson (1948)	0.5477	0.74
Eifler and Schrimpf (1992)	0.5	0.7143
Schumann and Gerz (1995)	0.5477	0.74

Table 3: Summary of model setup parameters.

Δx, Δy	0.1 m
Δt	0.01 s
Bed slope	4.2×10^{-4}
Bed roughness	8×10^{-4} m
h_0	0.39 m
$\bar{U}$	0.51 m/s
d	160×10^{-6} m
ρ_s	2650 kg/m^3
F_{morph}	10
ϕ	0.4

Table 4: Summary of numerical experiments. SIS: Sediment-induced stratification. NSS: No sediment stratification. C01-A: Canuto et al. (2001) Model A. C01-B: Canuto et al. (2001) Model B. G88: Galperin et al. (1988). MA48: Munk and Anderson (1948). ES92: Eifler and Schrimpf (1992). SG95: Schumann and Gerz (1995).

Experiment	Stratification	Turbulence length scale method	Stability functions	Erosion	E_0 $(kg/m^2/s)$	τ_{ce} (N/m^2)
S1A	SIS	ω	C01-A	Eq. 19	0.0082	0.17
S1B	SIS	ω	C01-A	Eq. 19	0.012	0.17
S1C	SIS	ω	C01-A	Eq. 19	0.0082	0.26
S1D	SIS	ω	C01-A	Eg. 19	0.0082	0.10
S1V	SIS	ω	C01-A	Eq. 20		
N1A	NSS	ω	C01-A	Eq. 19	0.0082	0.17
S2A	SIS	ε	C01-A	Eq. 19	0.0082	0.17
S2B	SIS	ε	C01-A	Eq. 19	0.012	0.17
S2D	SIS	ε	C01-A	Eg. 19	0.0082	0.10
N2B	NSS	ε	C01-A	Eq. 19	0.012	0.17
S3A	SIS	Algebraic	G88	Eq. 19	0.0082	0.17
S4A	SIS	ω	C01-B	Eq. 19	0.0082	0.17
S5A	SIS	ω	MA48	Eq. 19	0.0082	0.17
S6A	SIS	ω	ES92	Eq. 19	0.0082	0.17
S7A	SIS	ω	SG95	Eq. 19	0.0082	0.17

Table 5: Friction velocities upstream of the trench found analytically and from the different numerical experiments.

Case	$u_\star$(cm/s)
Analytical	4.0
S1A	3.92
S1B	3.87
S1C	3.94
S1D	3.86
S1V	3.41
N1A	3.97
S2A	3.65
S2B	3.59
S2D	3.58
N2B	3.71
S3A	3.21
S4A	4.02
S5A	4.01
S6A	4.02
S7A	3.99

Table 6: Brier Skill Scores for the different numerical experiments for the 3 trenches of different initial slopes S

Case	$S = 1/3$	$S = 1/7$	$S = 1/10$
S1A	0.9838	0.9499	0.9850
S1B	0.9048	0.9710	0.9443
S1C	0.8637	0.7579	0.8561
S1D	0.8568	0.9251	0.8834
S1V	0.7012	0.8046	0.7483
N1A	0.9503	0.9949	0.9807
S2A	0.6120	0.4134	0.5618
S2B	0.7631	0.5351	0.6679
S2D	0.7837	0.5519	0.6495
N2B	0.9173	0.8971	0.9002
S3A	0.7451	0.6392	0.7090
S4A	0.9836	0.9644	0.9899
S5A	0.9445	0.9855	0.9699
S6A	0.9399	0.9837	0.9670
S7A	0.9577	0.9898	0.9799

Figure 1: Two-dimensional sketch of the sediment model layered structure. Three bed layers are represented here. The active layer is of thickness δ_a and always part of the top bed layer. Changes in bed location are computed following equation 22 and results from vertical exchange between the bed and the suspended load via erosion E and deposition D.

Figure 2: Sketch of the trench setup in the 30 m long, 0.5 m wide flume. The dashed vertical lines show the locations at which velocity and suspended sediment concentration profiles were measured.

Figure 3: Velocity profiles (top) and suspended sediment concentration profiles (bottom) obtained with or without sediment-induced stratification.

Figure 4: Velocity profiles (top) and suspended sediment concentration profiles (bottom) obtained for experiment S1A $d = 160\mu m$ (black) and $d = 120\mu m$ (red). The circles represent the data of van Rijn (1987).

Figure 5: Trench migrations with or without sediment-induced suspension for trenches with initial slopes of 1/3 (top), 1/7 (middle), and 1/10 (bottom). The circles show the data, and the lines numerical results. Black solid: case S1A; grey solid: case N1A; black dashed: case S2B; grey dashed: case N2B.

Figure 6: Velocity profiles (top) and suspended sediment concentration profiles (bottom) obtained using equation 19 with $E_0 = 0.0082kg/m^2/s$ and $\tau_{ce} = 0.17N/m^2$ (experiment S1A) (black) or equation 20 (experiment S1V). The circles are the data of van Rijn (1987).

Figure 7: Trench migrations for different erosion approaches for trenches with initial slopes of 1/3 (top), 1/7 (middle), and 1/10 (bottom). Circles: experimental data; black solid: bathymetry after 15 hours for experiment S1A; grey solid: bathymetry after 15 hours for experiment S1V; dashed grey: bathymetry after 1.5 hours for experiment S1V.

Figure 8: Velocity profiles (top) and suspended sediment concentration profiles (bottom) obtained for different values of E_0 and τ_{ce}. Solid black: $E_0 = 0.0082kg/m^2/s$ and $\tau_{ce} = 0.17N/m^2$ (experiment S1A); solid red: $E_0 = 0.012kg/m^2/s$ and $\tau_{ce} = 0.17N/m^2$ (experiment S1B); solid blue: $E_0 = 0.0082kg/m^2/s$ and $\tau_{ce} = 0.26N/m^2$ (experiment S1C); dashed blue: $E_0 = 0.0082kg/m^2/s$ and $\tau_{ce} = 0.10N/m^2$ (experiment S1D). The circles are the data of van Rijn (1987).

Figure 9: Trench migrations for different values of E_0 and τ_{ce} for trenches with initial slopes of 1/3 (top), 1/7 (middle), and 1/10 (bottom). Circles: experimental data; black solid: $E_0 = 0.0082kg/m^2/s$ and $\tau_{ce} = 0.17N/m^2$ (experiment S1A); black dashed: $E_0 = 0.012kg/m^2/s$ and $\tau_{ce} = 0.17N/m^2$ (experiment S1B); black dot-dashed: $E_0 = 0.0082kg/m^2/s$ and $\tau_{ce} = 0.26N/m^2$ (experiment S1C); black dotted: $E_0 = 0.0082kg/m^2/s$ and $\tau_{ce} = 0.10N/m^2$ (experiment S1D); grey solid: experiment N1A.

Figure 10: Trench migrations for increasing values of E_0 and τ_{ce} for the $k - \varepsilon$ model for trenches with initial slopes of 1/3 (top), 1/7 (middle), and 1/10 (bottom). Circles: experimental data; black solid: $E_0 = 0.0082kg/m^2/s$ and $\tau_{ce} = 0.17N/m^2$ (experiment S2A); black dashed: $E_0 = 0.012kg/m^2/s$ and $\tau_{ce} = 0.17N/m^2$ (experiment S2B); black dot-dashed $E_0 = 0.0082kg/m^2/s$ and $\tau_{ce} = 0.10N/m^2$ (experiment S2D).

Figure 11: Velocity profiles (top) and suspended sediment concentration profiles (bottom) for different turbulence models. Solid black: $k - \omega$ model; red: $k - \varepsilon$ model; blue: one-equation k model; dashed black: case N1A; circles: experimental data.

Figure 12: Trench migrations for different turbulence models for trenches with initial slopes of 1/3 (top), 1/7 (middle), and 1/10 (bottom). Circles: experimental data; solid black: $k - \omega$ model; dahed black: $k - \varepsilon$ model; grey solid: one-equation k model.

Figure 13: Velocity profiles (top) and suspended sediment concentration profiles (bottom) for different stability functions. Circles: experimental data; black solid: Canuto et al. (2001) Model A; grey solid: Canuto et al. (2001) Model B; dashed blue: Munk and Anderson (1948); dashed red: Eifler and Schrimpf (1992); dashed green: Schumann and Gerz (1995); dashed black: case N1A.

Figure 14: Trench migrations for different stability functions for trenches with initial slopes of 1/3 (top), 1/7 (middle), and 1/10 (bottom). Circles: experimental data; black: Canuto et al. (2001) Model A; grey: Canuto et al. (2001) Model B; blue: Munk and Anderson (1948); red: Eifler and Schrimpf (1992); green: Schumann and Gerz (1995).

Figure 15: Top: Non-dimensional bed shear stress across the trench for the $k-\omega$ model (black) and $k-\varepsilon$ model (grey). Bottom: Erosion (solid) and deposition (dashed) across the trench for the $k-\omega$ model (black) and $k-\varepsilon$ model (grey).

Figure 16: Assessment of equation 28 at the five locations across the trench by plotting the left-hand side term $T(\omega)$ (solid) and the right-hand side term (dashed).

Figure 1

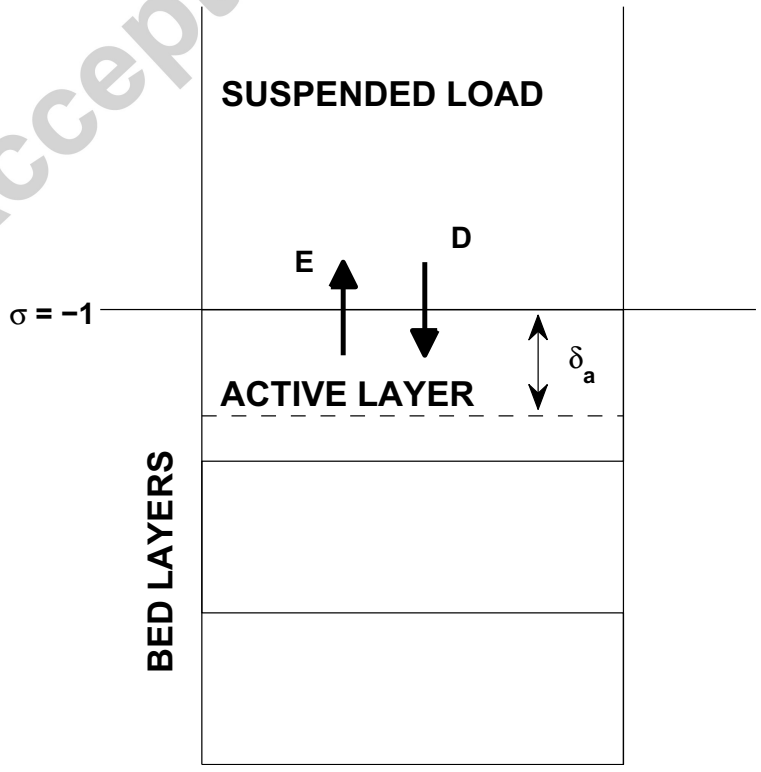

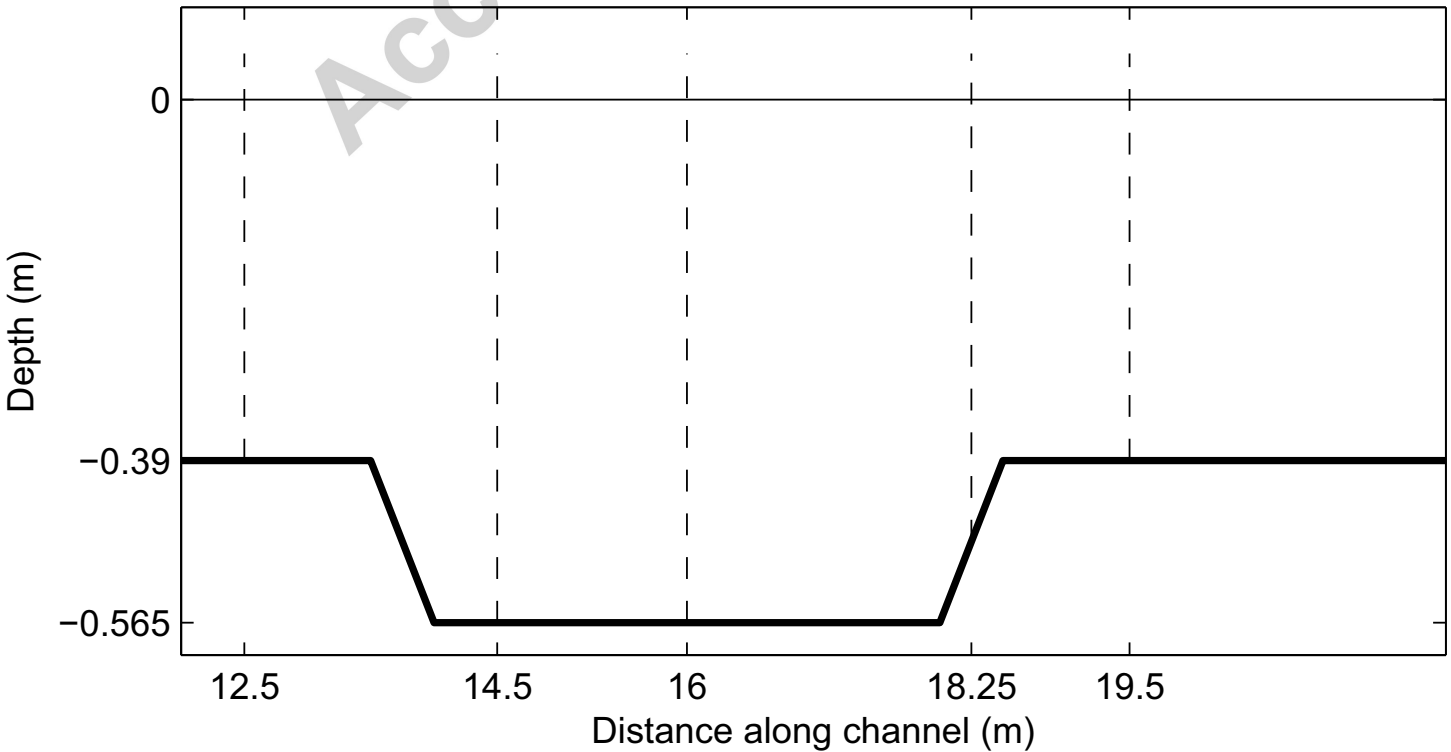

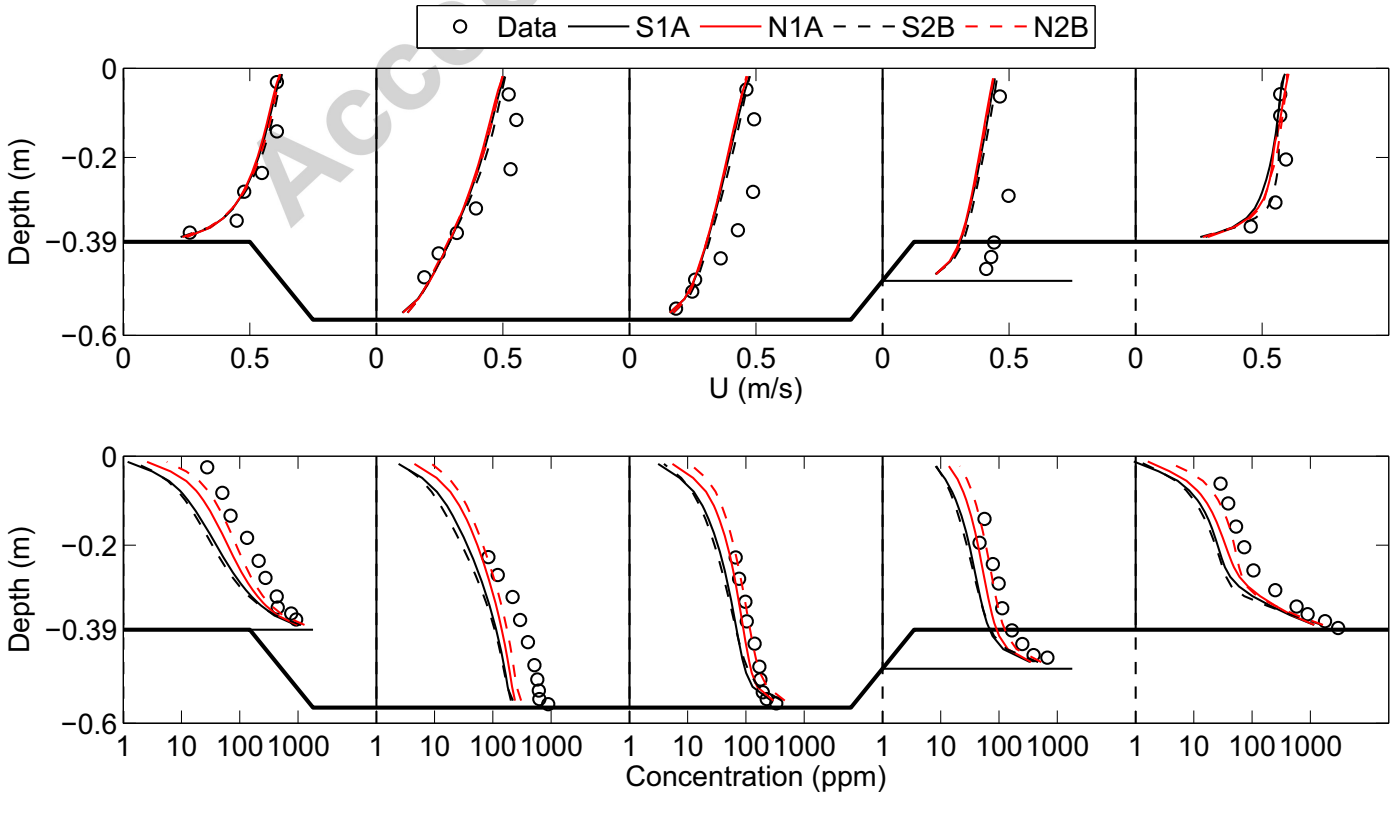

Figure 4

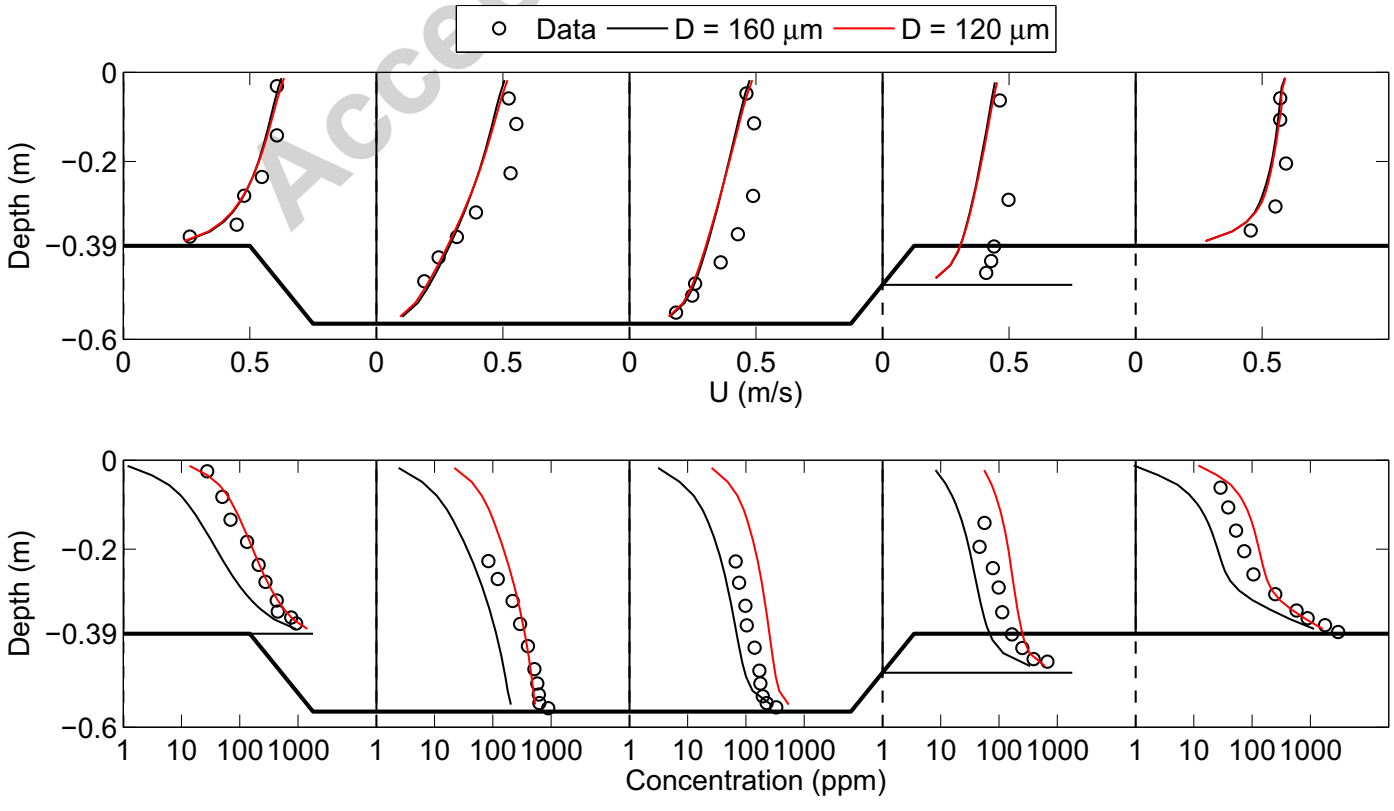

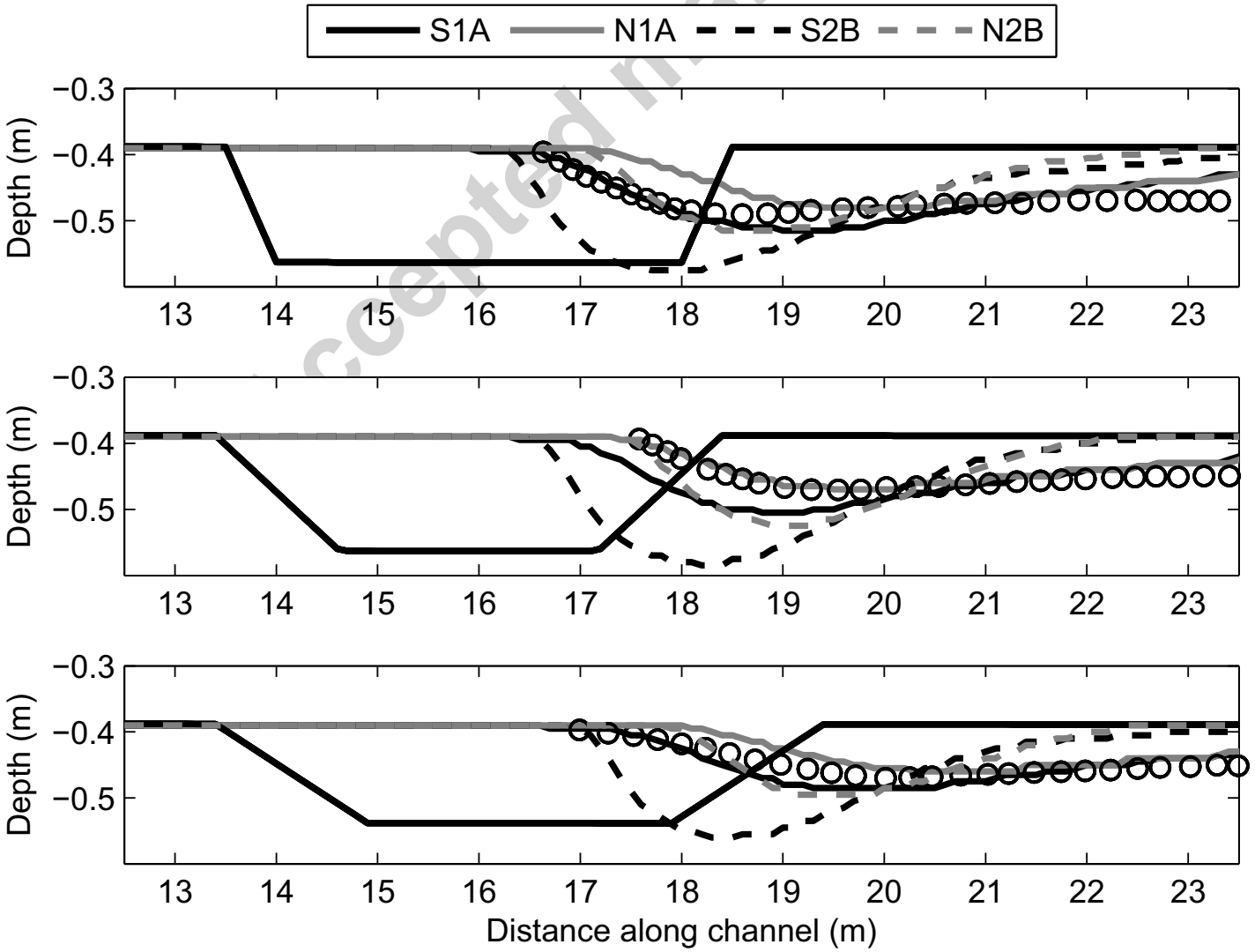

Figure 6

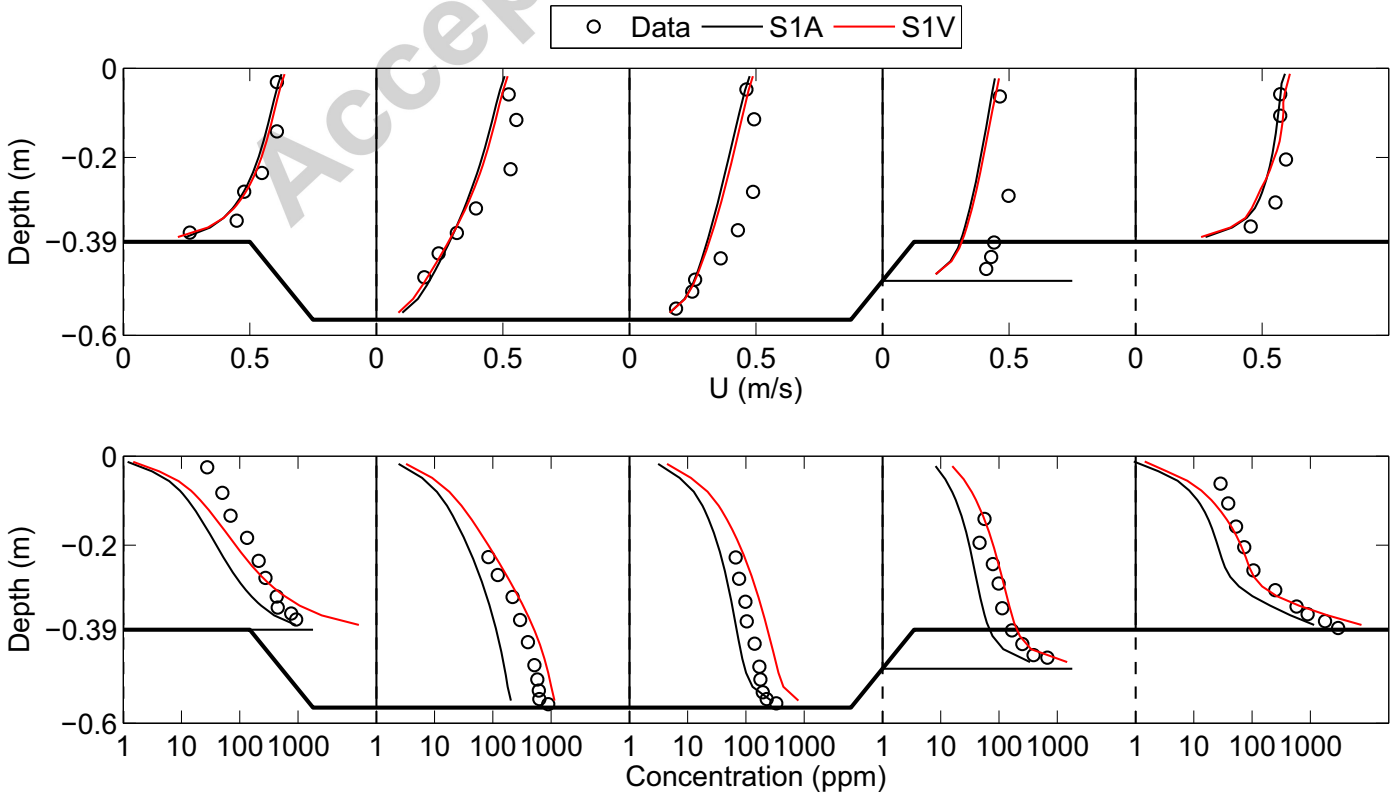

Figure 7

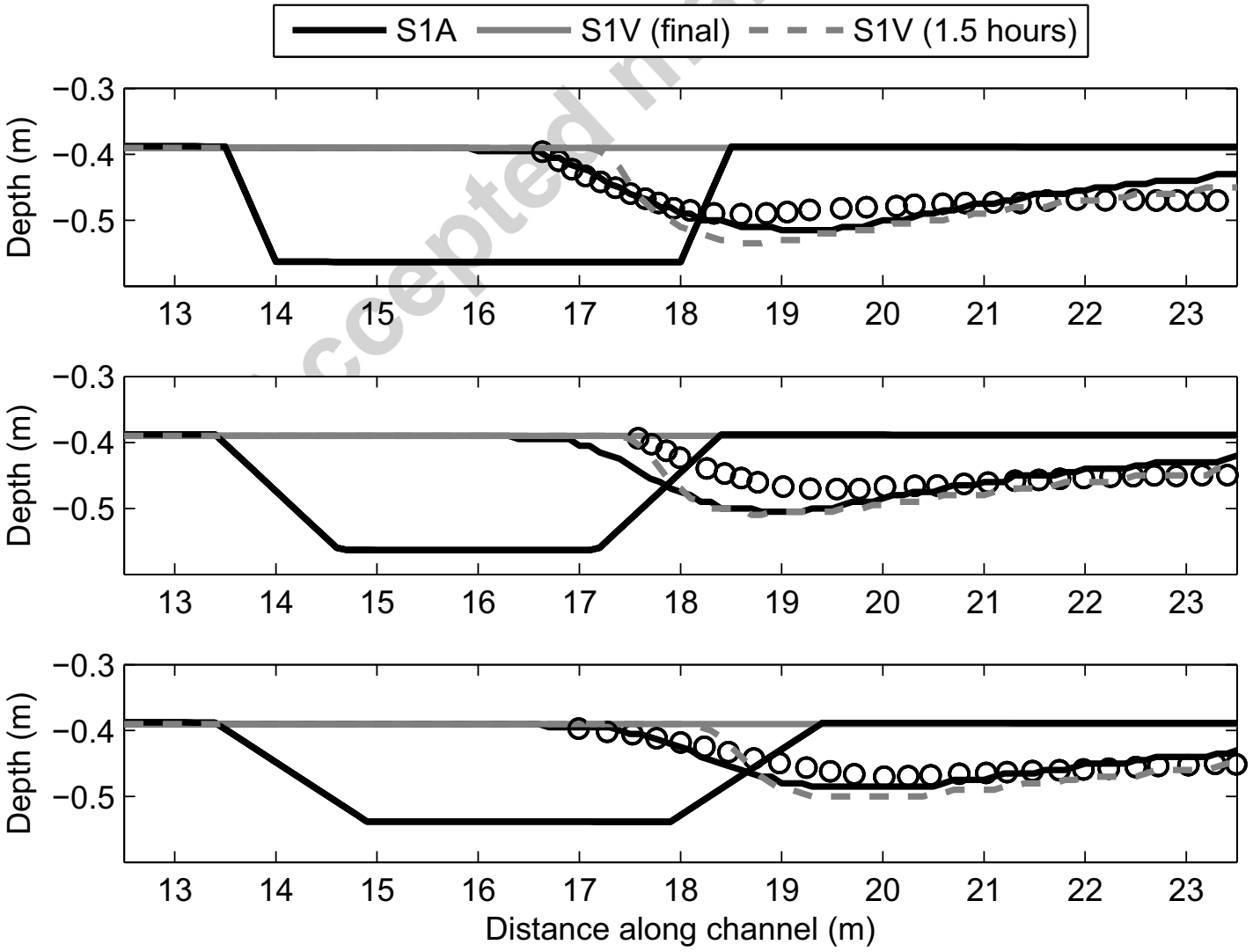

Figure 8

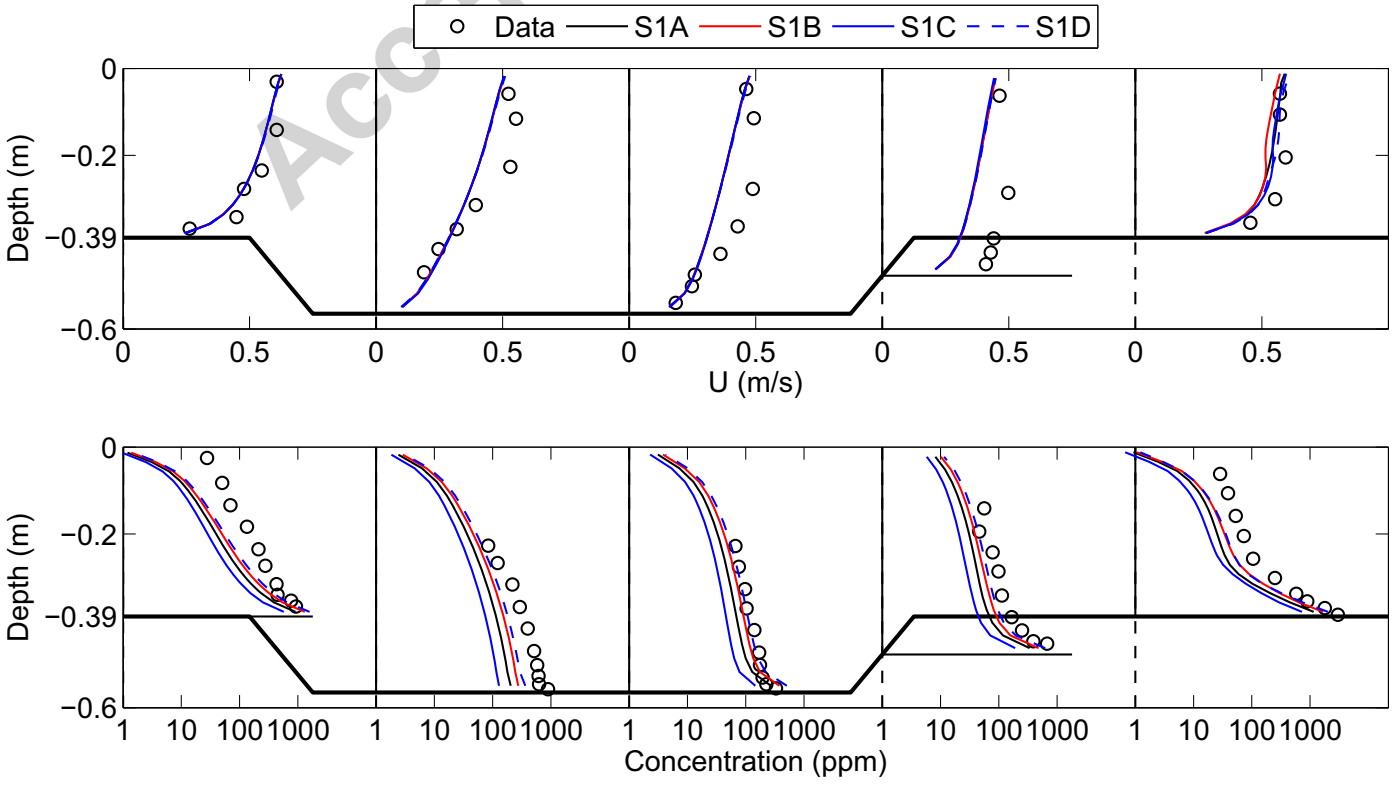

Figure 9

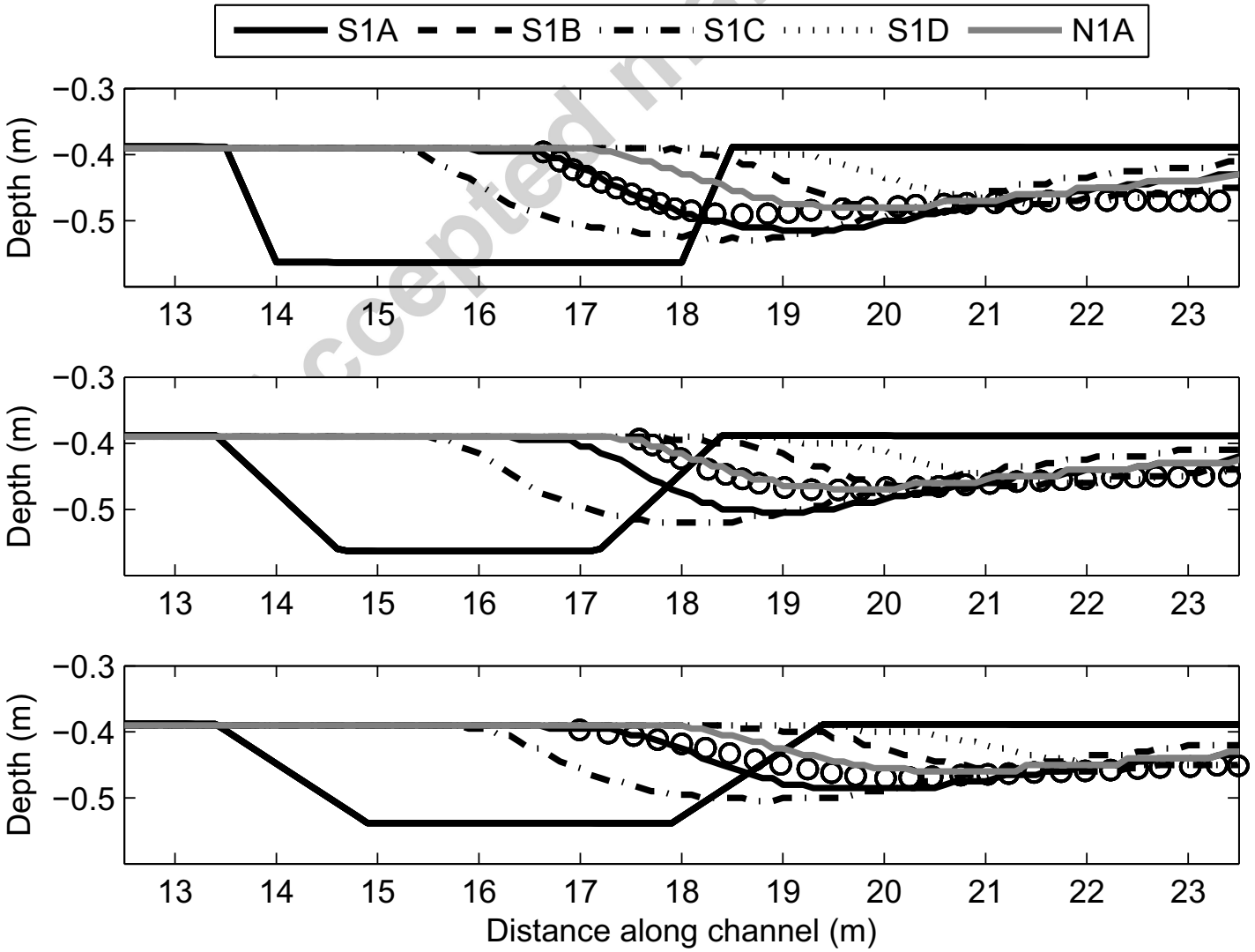

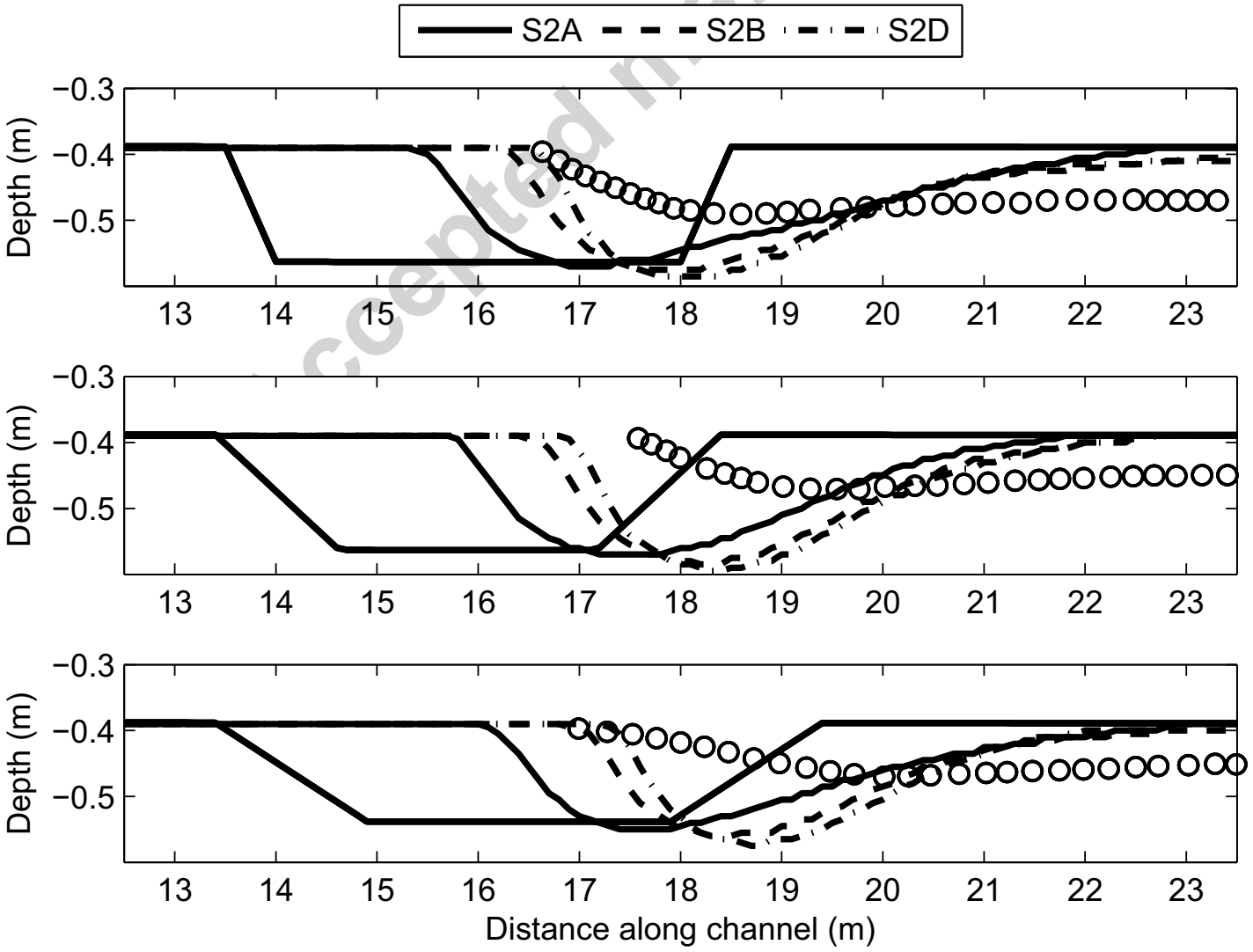

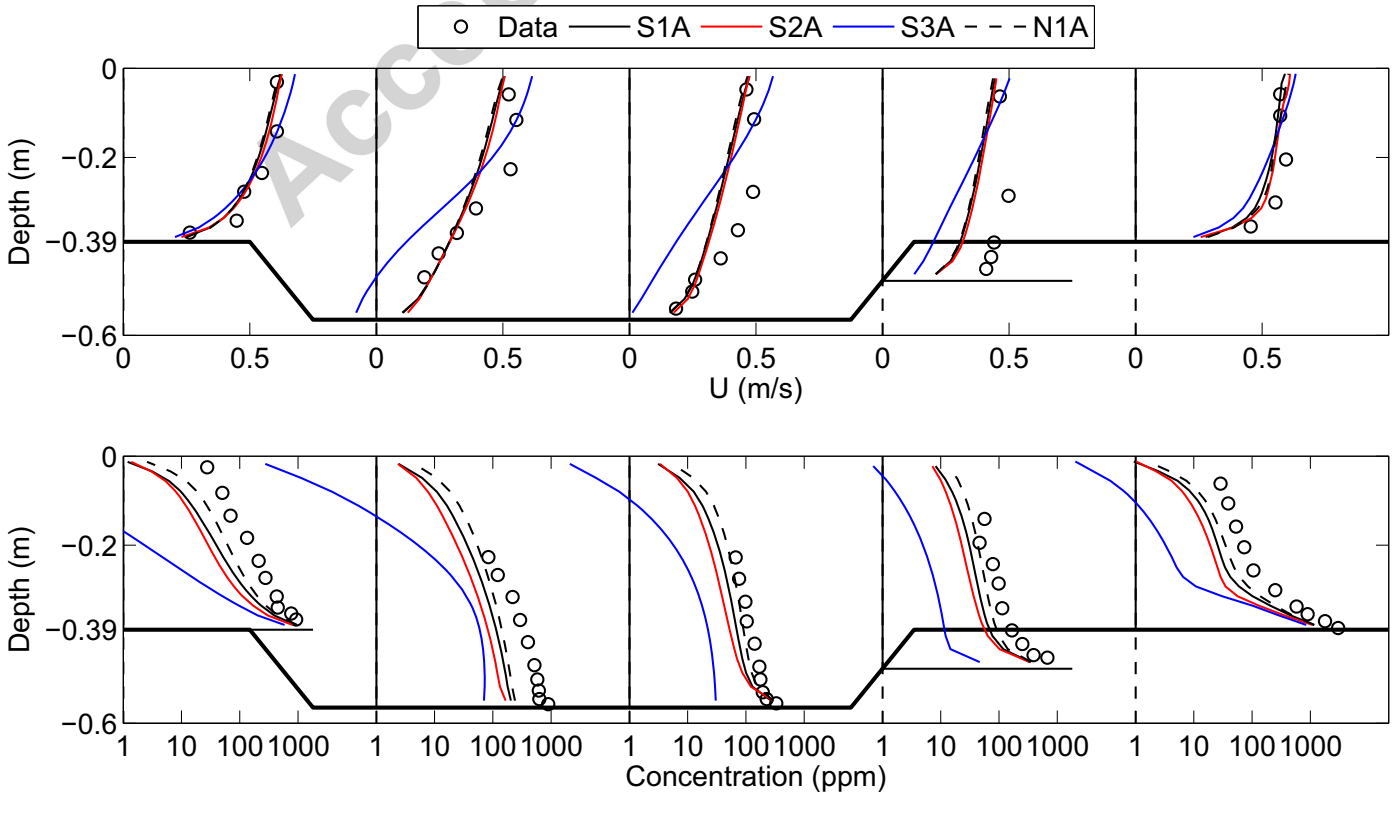

Figure 12

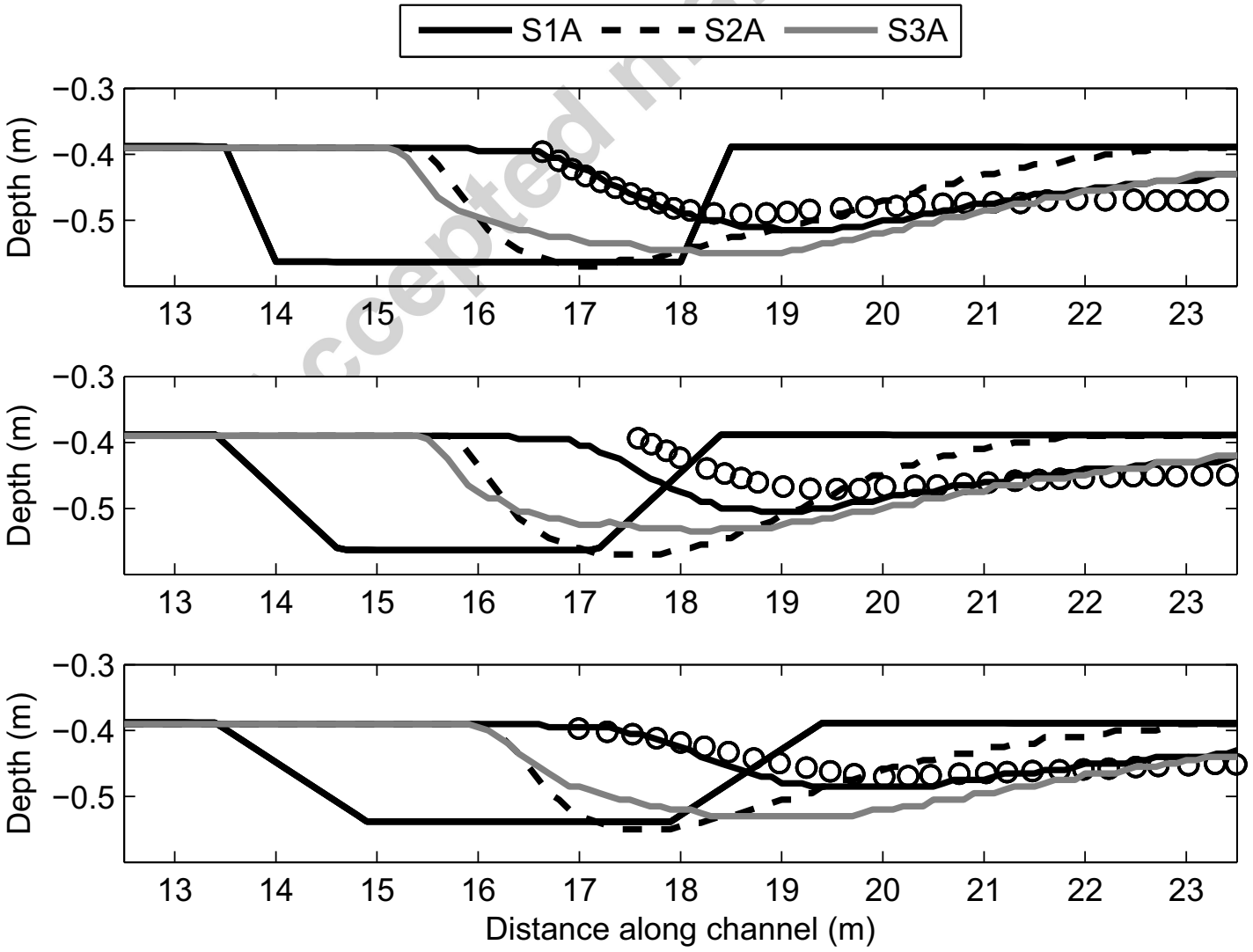

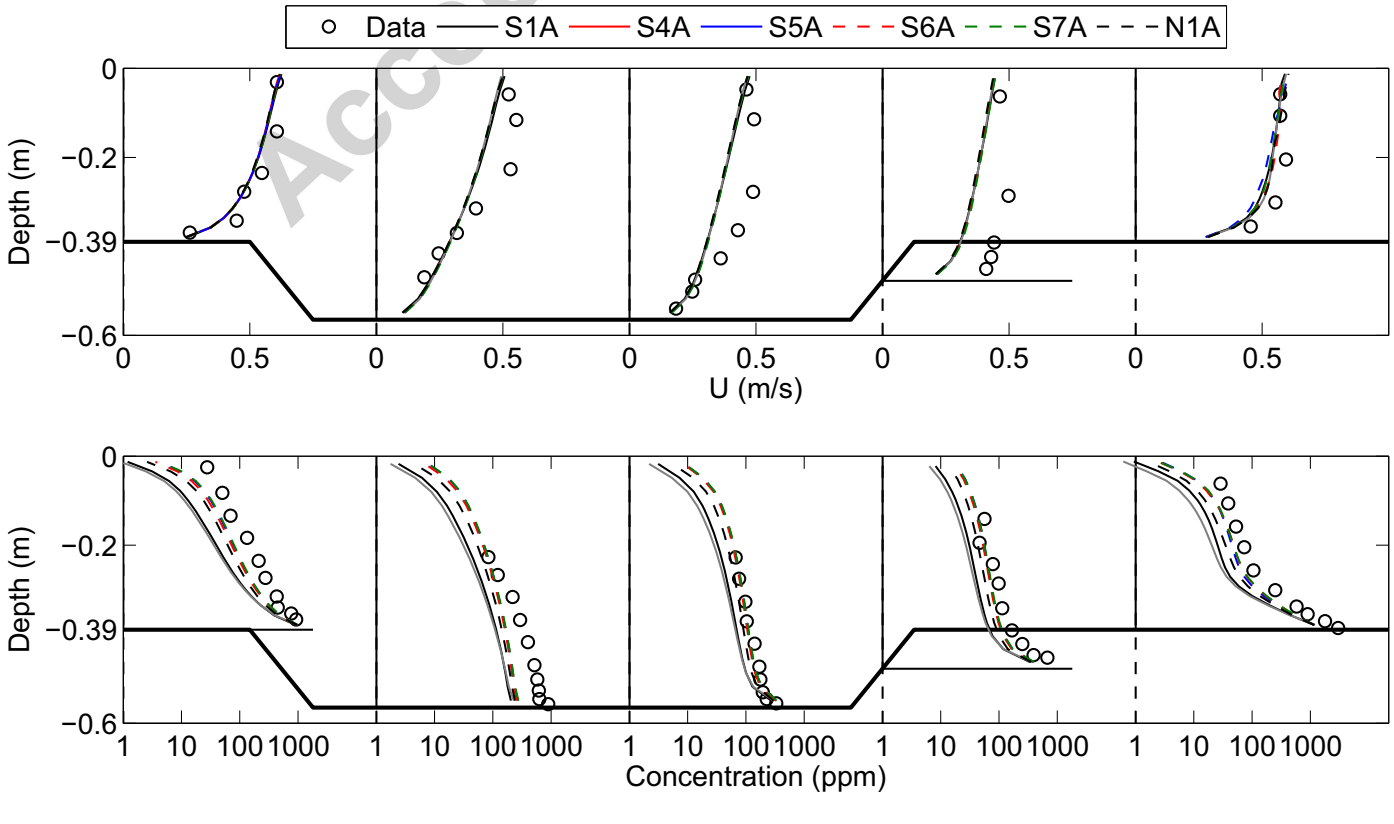

Figure 14

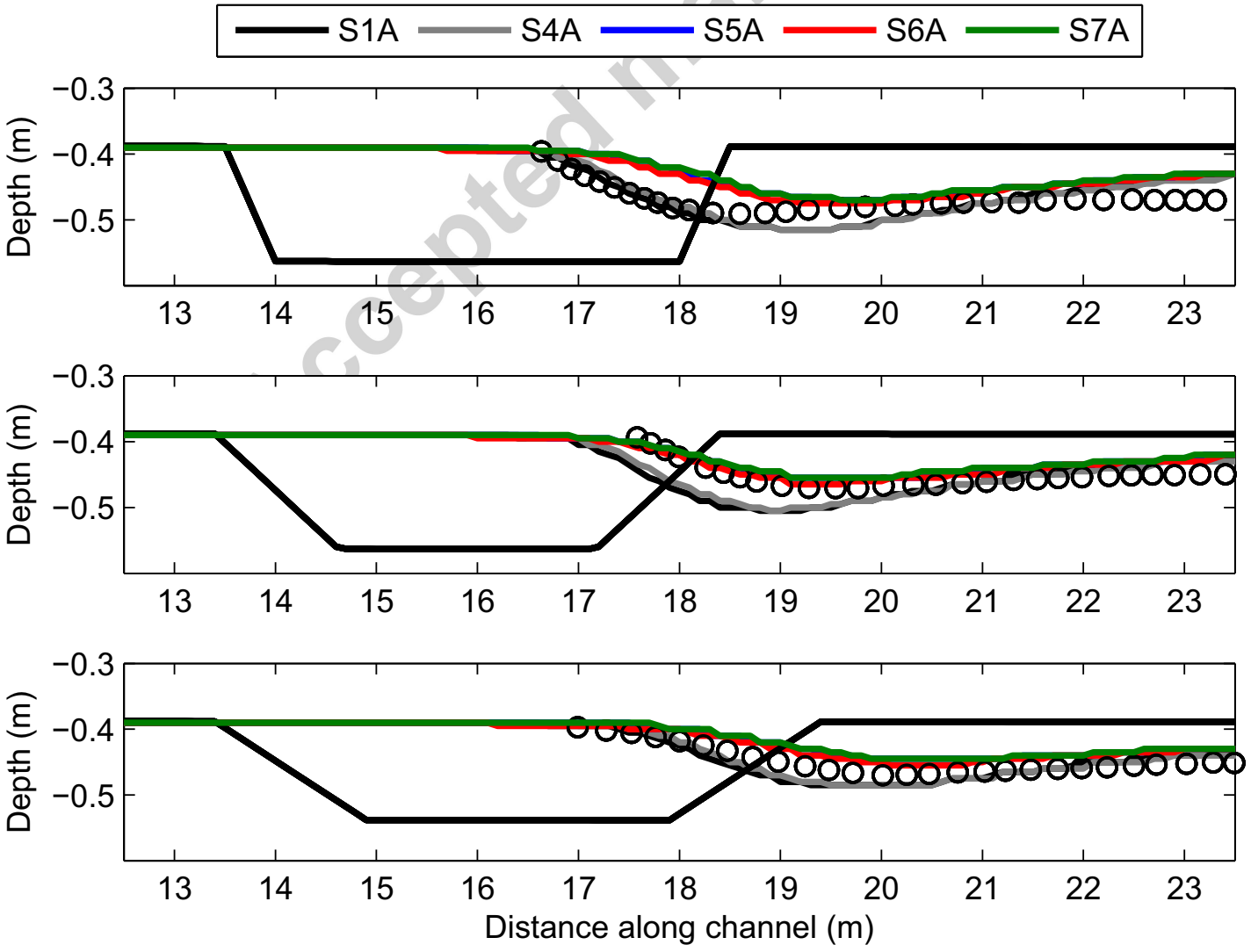

Figure 15

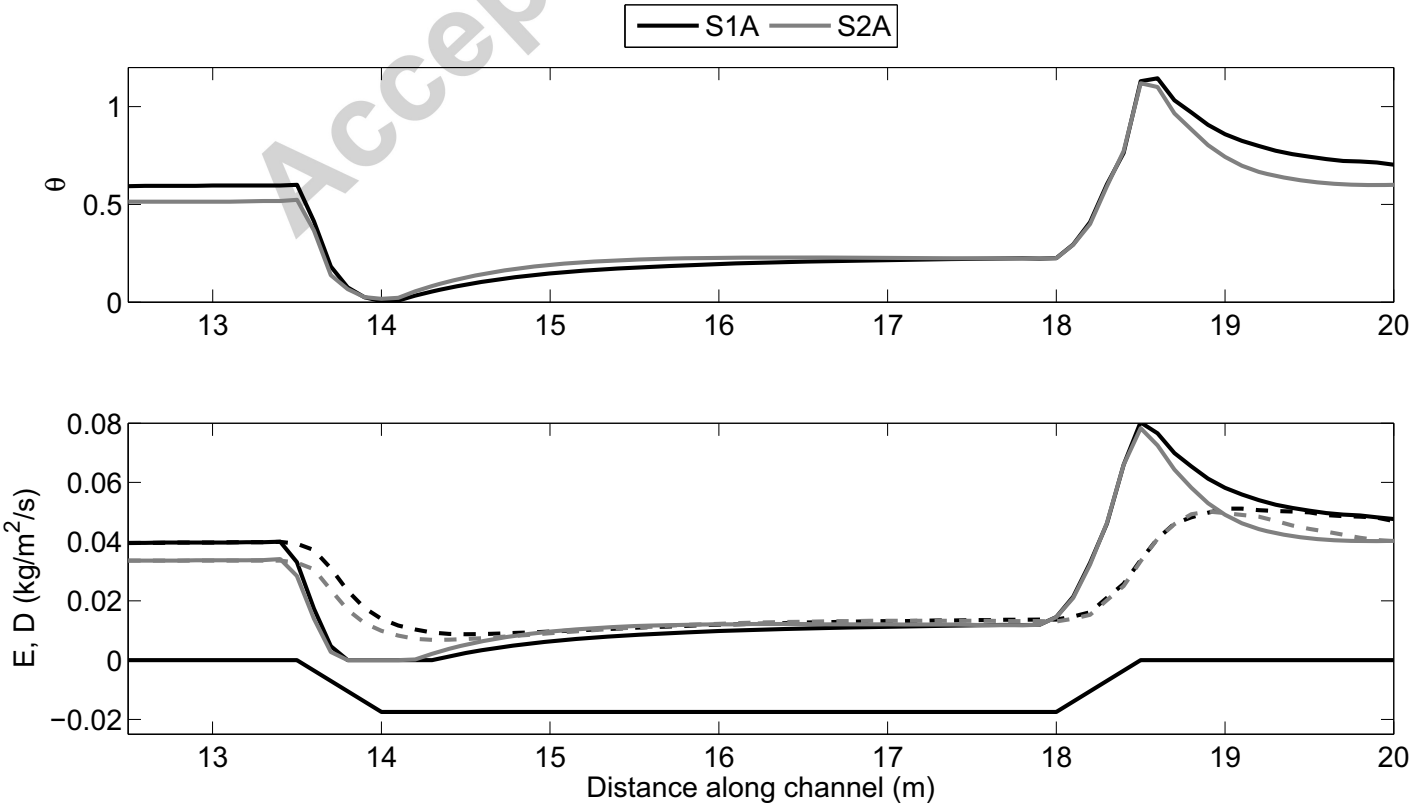

Figure 16

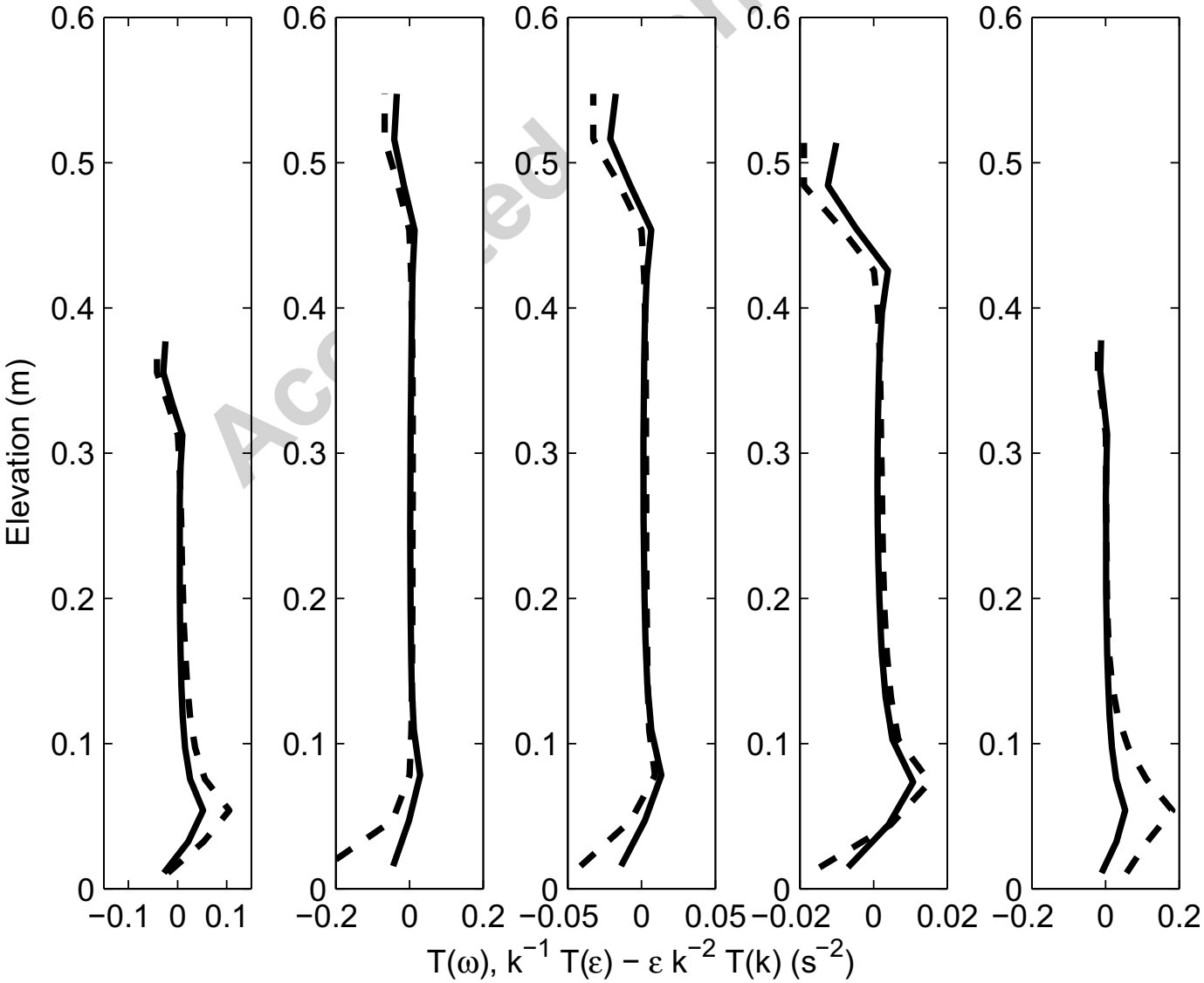

- We model suspended sediment concentrations and sediment bed evolution.
- We investigate the impact of several modelling approaches on numerical results.
- A good representation of the sediment size distribution is important.
- The parameterization of sediment erosion has the most dramatic effect.
- The choice of turbulence model also impacts numerical results.